Thermodynamic Uncertainty Relation in Superconducting Circuits

bachelor's thesis

presented by

Aristid Großmann

under the supervision of

Prof. Dr. Fabian Hassler

and

Prof. Dr. Mario Berta

Institute for Quantum Information

05.08.2025

Abstract

In many applications of superconducting circuits, the precision of current and voltage under thermal noise is of central importance. In the overdamped limit, the thermodynamic uncertainty relation (TUR) captures a fundamental trade-off between entropy production and precision of the accumulated voltage. In this work, we prove the TUR for systems with a periodic current-phase relation (CPR) and investigate the conditions for saturation. We further conjecture a tighter bound than the TUR for inversion-symmetric CPRs, formulated in terms accessible via the I-V curve of the system. We closely investigate the saturation of the TUR for two example systems of technological importance, namely the Josephson junction and the sawtooth ratchet.

Contents

Chapter 1

Introduction

In many applications of superconducting circuits, the precision of current and voltage under thermal noise is of central importance. The Josephson Junction (JJ) forms the fundamental building block of superconducting circuits [4]. In the overdamped regime, where resistive dissipation dominates over capacitive effects, JJs exhibit highly stable and reproducible voltage-frequency locking. This property makes them especially well-suited for use in metrology as voltage standards [23, 22]. However, thermal noise limits the precision of the integrated voltage in practical settings. In the overdamped limit, the thermodynamic uncertainty relation (TUR) formalizes the intuition that achieving higher precision comes at an energetic cost, by placing a universal bound on the precision of the accumulated voltage in terms of entropy production [12, 21]. This makes the TUR a powerful theoretical tool for understanding the impact of thermal noise on the precision of superconducting circuits. In this thesis, we investigate how the TUR manifests in overdamped superconducting systems, focusing specifically on periodic current-phase relations (CPRs), such as those found in JJs.

We start by closely examining the JJs CPR and the resulting voltage-frequency relation in Sec. 2.1 while neglecting thermal noise. We continue by deriving a simple model of thermal fluctuations as Gaussian white noise in Sec. 2.2, consistent with predictions from statistical physics. Combining the insights gained in both sections, we formulate the overdamped Langevin equation for the integrated voltage, which corresponds to the phase φ. This is is the common framework to describe overdamped systems subjected to thermal noise. In Sec. 2.3, we then formulate the TUR in terms of the uncertainty product $\tilde{\mathcal{Q}}$, which quantifies the tradeoff between precision and entropy production.

In Ch. 3, we explicitly calculate $\tilde{\mathcal{Q}}$ in the long-time limit by expressing the phase in terms of first passage times (FPTs). Leveraging the central limit theorem then allows us to express $\tilde{\mathcal{Q}}$ in terms of the mean and the variance of the FPT. In Sec. 3.2 we calculate the mean and the variance by solving the Backward Kolmogorov Equation, which concludes our calculation. Leveraging our analytical expressions, we prove the TUR in Sec. 3.3 for overdamped systems with periodic CPRs.

In Sec. 4.1, we analytically derive the conditions for TUR saturation and interpret them. We further conjecture a tighter bound than the TUR for inversion-symmetric CPRs, formulated in terms accessible via the I-V curve of the system. We continue to closely investigate the saturation of the TUR for two example systems of technological importance, namely the JJ and the sawtooth ratchet. The latter is of particular interest, since the sawtooth potential exhibits non-reprocity and even ideal diode-like behavior for specific parameterizations.

Chapter 2

Noise in Superconducting Circuits

The Josephson Junction is the core component of superconducting electronics, enabling phenomena such as quantum coherence and dissipationless current flow. Its unique nonlinear behavior, governed by the Josephson relations, gives rise to a rich dynamical structure that underpins applications ranging from voltage standards [23, 22] to qubits [13] and SQUIDs [6]. In this chapter, we introduce the JJ's fundamental physics, develop its dynamical description using the RCSJ model, and analyze the phase evolution in the overdamped regime. This sets the stage for understanding noise and precision limits in superconducting circuits.

2.1 Josephson Junction

The JJ forms the fundamental building block of superconducting circuits [4]. It consists of two superconductors separated by a thin insulating barrier. Bound pairs of electrons (also called Cooper pairs) can tunnel across the barrier, which is the Josephson effect. The two Josephson relations read

$$I(t) = I_\mathrm{c} \sin(\varphi(t)) \tag{2.1}$$

$$V(t) = \frac{\hbar}{2e} \frac{\mathrm{d}\varphi}{\mathrm{d}t} \tag{2.2}$$

where e is the elementary charge and $\hbar$ is the reduced Planck constant [23]. The first equation (also called the first Josephson relation or weak-link current-phase relation) expresses the current I over the JJ as a function of its phase φ and the junction's critical current I_c. The second equation (also referred to as the second Josephson relation) links the voltage V over the junction to its phase. The JJ is classically described by the Resistively Capacitance Shunted Junction (RCSJ) model

$$I_0 = C_\mathrm{J} \frac{\mathrm{d}V}{\mathrm{d}t} + I_\mathrm{c} \sin(\varphi(t)) + \frac{V(t)}{R} \tag{2.3}$$

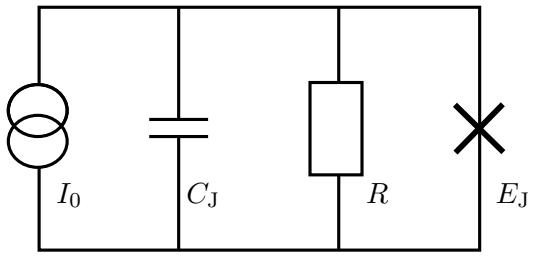

Figure 2.1: Equivalent circuit of a JJ in analogy to [23] with external bias current I_0, the capacitance C_J and resistance R. The critical current is related to the Josephson energy via $I_\mathrm{J} = 2eE_\mathrm{c}/\hbar$.

where I_0 is an external bias current, C_J is the junction's capacitance, and R is the junction's resistance, also referred to as the normal resistance [23]. The circuit diagram of the corresponding circuit is shown in Fig. 2.1. The McCumber-Stewart parameter $\beta_\mathrm{c} = 2eR^2 I_\mathrm{c} C/\hbar$ characterizes the damping strength. For $\beta_\mathrm{c} > 1$, the JJ's I–V curve shows hysteresis, while for $\beta_\mathrm{c} \ll 1$, the JJ behaves in a non-latching, overdamped manner. For instance, JJ applications in voltage standards require $\beta_\mathrm{c} \ll 1$: the precise, reproducible voltage steps that are needed for voltage standards are only achievable when the I–V curve is smooth and free of hysteresis. In the overdamped limit $\beta_\mathrm{c} \ll 1$, where resistive dissipation dominates over capacitive effects, the JJ's phase dynamics are described by the first-order nonlinear Ordinary Differential Equation (ODE)

$$\frac{\hbar}{2e}\frac{\mathrm{d}\varphi}{\mathrm{d}t} = RI_0 + RI_\mathrm{c}\sin(\varphi(t)) \,. \tag{2.4}$$

Introducing the variables $i_0 = I_0/I_\mathrm{c}$ and $\tau = t/t_0$, where $t_0 = \hbar/(2eRI_\mathrm{c})$ is the time scale on which initial conditions decay, enables us to express the phase dynamics in dimensionless quantities

$$\frac{\mathrm{d}\varphi}{\mathrm{d}\tau} = i_0 - \sin(\varphi) = f(\varphi) := -\frac{\mathrm{d}U}{\mathrm{d}\varphi} \,, \tag{2.5}$$

where f is interpreted as a drift force, expressed by the gradient of the tilted washboard potential $U(\varphi) = -i_0\varphi - \cos(\varphi)$ [23]. The term $-\cos(\varphi)$ is interpreted as an energy-phase-relation (EPR), which is related to the JJ's CPR via the derivative $-d\cos(\varphi)/d\varphi = \sin(\varphi)$. Examining the JJ's phase dynamics in terms of this potential allows for a more intuitive understanding, see Fig. 2.2: The JJ's phase dynamics are analogous to a particle moving in a tilted washboard potential. For external currents smaller than the critical current ($i_0 < 1$), the potential retains local minima. In the overdamped limit, where the particle lacks inertia, escape from these local minima is impossible [1]. When the the external current equals the critical current ($i_0 = 1$), the local minima turn into saddle points. If the bias exceeds the critical current ($i_0 > 1$), the tilt is large enough so that all local minima disappear, and the particle runs down the slope indefinitely in an oscillatory manner, resulting in a net voltage across

[1] Noise-assisted escape will be addressed in later sections.

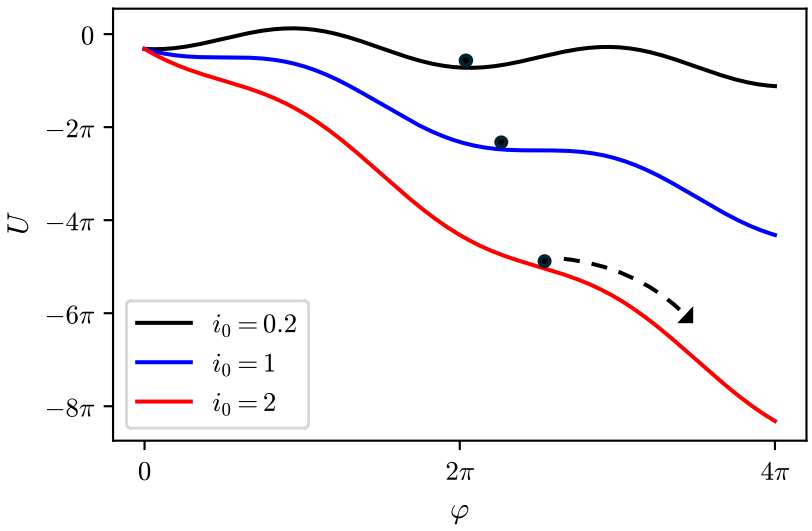

Figure 2.2: Tilted washboard potential potential $U(\varphi) = -i_0\varphi - \cos(\varphi)$ for different currents (tilts) $i_0 = I_0/I_c$. If the external current is smaller than the critical current, the potential exhibits local minima, which trap the "phase particle". If the external current exceeds the critical current, the local minima disappear, and the "phase particle" runs down the slope forever in an oscillatory manner, which results in a net voltage across the JJ.

the JJ. Because of the periodicity of the driving force, the phase then monotonically grows in 2π-increments. Indeed, for $i_0 < 1$ after initial conditions decay on the time scale t_0, the phase settles into a stable minimum with $\varphi \mod 2\pi = \arcsin(i_0)$. For $i_0 > 1$, we solve Eq. (2.5) via separation of variables. The resulting integrals can be calculated via the tangent half-angle substitution. After substituting $\omega_0 = \sqrt{i_0^2 - 1}$, we obtain

$$\tan(\varphi/2) = \frac{\omega_0}{i_0} \tan\left(\frac{\tau - \tau_0}{2}\omega_0\right) + \frac{1}{i_0} ,$$

where τ_0 is given by the initial condition $\varphi(\tau_0) = \varphi_0$. For simplicity, we set the initial condition to $\varphi_0 = 0$ and $\tau_0 = 0$ throughout this thesis. Comparing both sides, we deduce that the phase is a running process in which φ increases by $\Delta\varphi = 2\pi$ over the period $T = 2\pi/\omega_0$. The average voltage is equal to the average over one oscillation period

$$\overline{v} = \frac{\overline{V}}{RI_c} = \frac{1}{T}\int_0^T d\tau \frac{\mathrm{d}\varphi}{\mathrm{d}\tau} = \frac{\varphi(T) - \varphi(0)}{T} = \frac{2\pi}{T} = \omega_0$$

for $i_0 > 1$ and $\overline{v} = 0$ for $i_0 < 1$. Plotting the average dimensionless voltage $\overline{v}$ with respect to the dimensionless current i_0, we obtain the I-V-curve of the JJ, see Fig. 2.3. Below the critical current, the JJ exhibits a zero-voltage state. In this state, it is possible to transmit the supercurrent I_0 without resistance. We thus recovered a defining property of a superconducting circuit. Above the

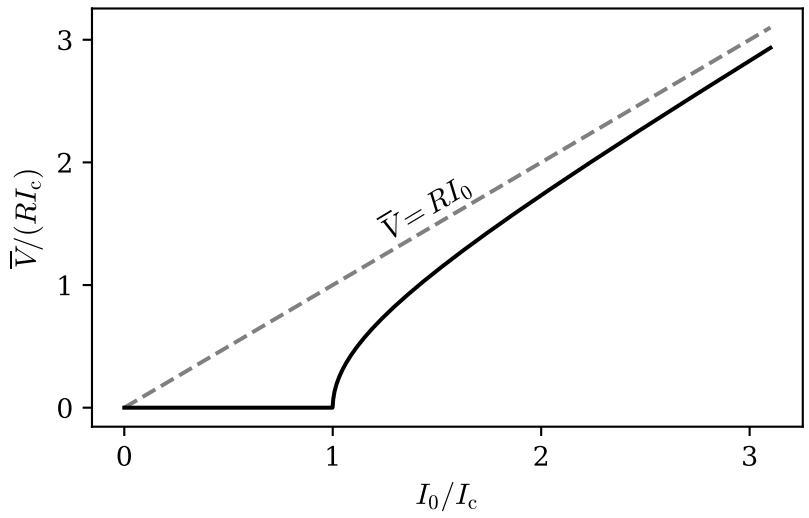

Figure 2.3: I-V-curve of the Josephson Junction. In the zero-voltage state $I_0 < I_c$, the supercurrent I_0 flows across the junction without resistance. In the finite-voltage state $I_0 > I_c$, the junction enters a resistive state. For bias currents much greater than the critical current, the junction behaves like an Ohmic resistor.

critical current, the junction enters a resistive state corresponding to a finite voltage. For bias currents much greater than the critical current, the JJ behaves like an Ohmic resistor. This property is crucial in later sections.

2.2 Thermal Noise of an Ohmic Resistor

According to the equipartition theorem, the expected energy in thermal equilibrium, associated with each quadratic degree of freedom equals $k_B T/2$, where k_B is the Boltzmann constant. Therefore, a purely deterministic circuit model as in Sec. 2.1 is inconsistent with predictions statistical physics. This motivates a statistical model which accounts for thermal fluctuations. Indeed, in reality the current bias is subject to noise $\delta I_R(t)$ due to thermal fluctuations. To account for this, we consider the circuit to be in thermal equilibrium with an idealized infinite heat bath at temperature T. Heat exchange between the circuit and the bath occurs through the circuit's resistance R, which is assumed to be constant. A simple yet effective way to model thermal fluctuations is to represent them as Gaussian white noise $\delta V_R(t) = R\delta I_R(t) = B\xi(t)$ where $\xi(t)$ is a stochastic process with mean $\langle \xi(t) \rangle = 0$ and correlation $\langle \xi(t)\xi(t') \rangle = \delta(t - t')$ [2] [21, 17] . The parameter B characterizes the strength of the noise and must be consistent with the equipartition theorem. To derive the consistent noise strength, we analyze a simple LR circuit, consisting of an Ohmic resistor R and

[2]The variance of $\xi(t)$ is ill-defined, with $\langle \langle \xi(t)^2 \rangle \rangle = \delta(0)$. This problem is covered in the next chapter.

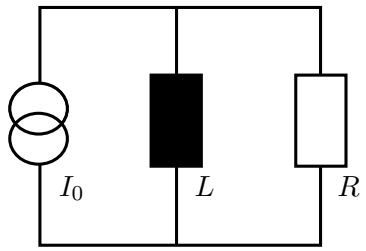

Figure 2.4: Circuit diagram of an LR-circuit with resistance R, inductance L and current bias I_0. For the calculations in this sections, the DC current bias is set to zero.

an inductance L. First, we aim to express the circuit dynamics in terms of the phase ϕ. The current-voltage relations of the respective components read

$$V_{\mathrm{R}} = RI_{\mathrm{R}} \tag{2.6}$$

$$V_{\mathrm{L}} = L\frac{\mathrm{d}I_{\mathrm{L}}}{\mathrm{d}t} \tag{2.7}$$

where I_{R} and V_{R} are the current and the voltage across the resistor, and I_{L} and V_{L} are the current and voltage across the inductance. According to Kirchhoff's rules, $I_{\mathrm{L}} - I_{\mathrm{R}} = 0$ and $V_{\mathrm{L}} + V_{\mathrm{R}} = 0$ (without thermal noise). Combining equations, we obtain

$$\begin{aligned} &\frac{\mathrm{d}I_{\mathrm{L}}}{\mathrm{d}t} + \frac{R}{L}I_{\mathrm{L}} = 0 \\ \rightarrow\ &I_{\mathrm{L}}(t) = I_{\mathrm{L}}(0)\exp\left(-\frac{R}{L}t\right) \end{aligned} \tag{2.8}$$

The expectation value of the circuit's energy in thermal equilibrium is equal to the energy stored inside a coil, which is given by

$$\langle E\rangle = \left\langle \frac{1}{2}LI_{\mathrm{L}}^2 \right\rangle \tag{2.9}$$

and must be equal to $k_{\mathrm{B}}T/2$ in equilibrium according to the equipartition theorem. However, without thermal noise, the current I_{L} converges to zero in the long-time limit, which is inconsistent with statistical physics. When accounting for voltage fluctuations due to thermal noise, the right-hand side (RHS) of Eq. (2.8) is no longer zero. Instead,

$$\frac{\mathrm{d}I_{\mathrm{L}}}{\mathrm{d}t} + \frac{R}{L}I_{\mathrm{L}} = \frac{B}{L}\tilde{\xi}(t). \tag{2.10}$$

Solving for the current I_{L} yields the general solution

$$\begin{aligned} I_{\mathrm{L}}(t) &= I_{\mathrm{L}}(0)\exp\left(-\frac{R}{L}t\right) + \int_0^t dt'\ \frac{B}{L}\xi(t')\exp\left(-\frac{R}{L}(t-t')\right) \\ &= \int_0^\infty dt'\ \frac{B}{L}\xi(t')\exp\left(-\frac{R}{L}(t-t')\right) \quad \text{in the long-time limit } t\to\infty. \end{aligned} \tag{2.11}$$

In the long-time limit, the expectation value of the system's energy is calculated by taking the ensemble average of the integrand and substituting the correlation function

$$\begin{aligned}\left\langle \frac{1}{2}LI_{\mathrm{L}}^2 \right\rangle &= \frac{L}{2}\lim_{t\to\infty}\int_0^t dt' \int_0^t dt'' \, \frac{B^2}{L^2}\exp\left(-\frac{R}{L}(2t-t'-t'')\right)\underbrace{\left\langle \xi(t')\xi(t'')\right\rangle}_{=\delta(\tau'-\tau'')} \\ &= \frac{B^2}{2L}\lim_{t\to\infty}\int_0^t dt' \, \exp\left(-2\frac{R}{L}(t-t')\right) \\ &= \lim_{t\to\infty}\frac{B^2}{4R}\left[1-\exp\left(-\frac{2R}{L}t\right)\right] \\ &= \frac{B^2}{4R} = \frac{k_{\mathrm{B}}T}{2} \quad \to B = \sqrt{2Rk_{\mathrm{B}}T}\,. \end{aligned} \tag{2.12}$$

Using the equipartition theorem in the last line and rearranging, we obtain the voltage fluctuations from an ohmic resistor $\delta V_{\mathrm{R}}(t) = \sqrt{2Rk_{\mathrm{B}}T}\xi(t)$ [21, 1]. This expression is also commonly referred to as Nyquist–Johnson noise, which is a fundamental result of the fluctuation-dissipation theorem [1, 23]. To obtain a general description of an overdamped circuit with a periodic CPR, we define a general CPR in analogy to the Josephson relations from Eq. (2.1) and Eq. (2.2)

$$I(t) = I_{\mathrm{c}}\frac{\mathrm{d}P}{\mathrm{d}\varphi} \tag{2.13}$$

$$V(t) = RI_{\mathrm{c}}t_0\frac{\mathrm{d}\varphi}{\mathrm{d}t}\,, \tag{2.14}$$

where $P(\varphi)$ is the corresponding EPR, I_{c} is the circuit's characteristic current [3], R is the circuit's resistance, and t_0 is the time scale on which initial conditions decay. Combining our result for the thermal noise strength of an Ohmic resistor with the insights gained from analyzing the JJ, we conclude that, in the overdamped limit and including thermal noise, the phase φ of any circuit whose CPR can be described by Eq. (2.13) and Eq. (2.14) is governed by an overdamped Langevin equation

$$RI_{\mathrm{c}}t_0\frac{\mathrm{d}\varphi}{\mathrm{d}t} = RI_0 - RI_{\mathrm{c}}\frac{\mathrm{d}P}{\mathrm{d}\varphi} + \sqrt{2Rk_{\mathrm{B}}T}\,\xi(t) \tag{2.15}$$

with the temperature T of the surrounding heat bath and the Gaussian white noise $\xi(t)$. The overdamped Langevin equation describes a Markovian (memoryless) stochastic process, which means that the phase's future evolution only depends on its current state and not its history. This property will become important in later chapters. After dividing both sides by RI_{c}, we can express the driving force of the process via the tilted periodic potential $U(\varphi) = -i_0\varphi + P(\varphi)$ with $i_0 = I_0/I_{\mathrm{c}}$. We obtain

$$t_0\frac{\mathrm{d}\varphi}{\mathrm{d}t} = -\frac{\mathrm{d}U}{\mathrm{d}\varphi} + \sqrt{\frac{2k_{\mathrm{B}}T}{RI_{\mathrm{c}}^2}}\,\xi(t)\,. \tag{2.16}$$

[3] The characteristic current can be set to the coefficient of the first harmonic of the CPR if the latter is finite. For the JJ, this quantity coincides with its critical current. Note however, that some EPRs involve infinite critical currents, such as the sawtooth ratchet, which is a topic in later chapters.

Note that, because the left-hand side (LHS) is dimensionless and the term under the square root is proportional to the thermal energy of the heat bath divided by the power consumption of the circuit, the dimension of the noise $\xi(t)$ is $[s^{-1/2}]$.

2.3 Thermodynamic Constraints on Precision

Many applications of superconducting circuits for high-precision technologies, most famously for quantum computing, but also ultra-sensitive magnetometers, amplifiers and sensors, pose tight constraints on precision and noise. Even small fluctuations in the system's degrees of freedom can lead to loss of coherence, readout errors, or degraded signal resolution. A simple measure of precision is given by the square of the coefficient of variation $\mathrm{CV}_\varphi^2 = \langle\langle\varphi^2\rangle\rangle/\langle\varphi\rangle^2$, where $\langle\varphi\rangle$ is the mean of the phase and $\langle\langle\varphi^2\rangle\rangle$ denotes its variance. To maximize precision, this ratio is desired to be kept as low as possible. Intuitively however, achieving higher precision comes at an energetic cost. In the overdamped limit, the TUR formalizes this trade-off between precision and thermodynamic cost by placing a universal bound on the precision of the phase

$$\frac{\langle\langle\varphi^2(t)\rangle\rangle}{\langle\varphi(t)\rangle^2}\Sigma_\varphi \geq 2k_\mathrm{B} \,, \tag{2.17}$$

where Σ_φ is the total entropy production up to time t [12, 21]. In this context, total entropy production can be interpreted as a measure of thermodynamic cost for maintaining the non-equilibrium steady state [21]. The TUR was first discovered as a lower bound for the trade-off between precision and irreversibility in the context of non-equilibrium bimolecular processes [2]. It was first proven for equilibrium steady-state currents in Markov jump processes in the long-time limit [7], where current fluctuations become Gaussian. Shortly after, it was proven to also hold for non-equilibrium steady-state currents on arbitrary time scales [14]. Additional analysis showed that for a system governed by an overdamped Langevin equation, such as our description of an overdamped circuit in Eq. (2.16), the TUR holds for arbitrary states on arbitrary time scales [9, 15]. In the case of a current bias, the entropy production rate in a steady state is determined by the average power dissipation into the heat bath with temperature T

$$\Sigma_\varphi = \int_0^t dt' \, \frac{I_0\langle V(t')\rangle}{T} \; = \frac{RI_0I_\mathrm{c}t_0}{T}\langle\varphi(t)\rangle \,, \tag{2.18}$$

where the relation between voltage and phase according to Eq. (2.14) was used in the last step. Substituting this expression for the total entropy production into the LHS of the TUR yields

$$\frac{\langle\langle\varphi^2(t)\rangle\rangle}{\langle\varphi(t)\rangle}\frac{RI_0I_\mathrm{c}t_0}{T} \geq 2k_\mathrm{B} \,. \tag{2.19}$$

The LHS of the TUR is commonly referred to as the uncertainty product $\mathcal{Q}(t)$ [21]. This quantity is closely analyzed in the next chapter.

Chapter 3

Thermodynamic Uncertainty Relation

The goal of this chapter is to explicitly calculate the LHS of the TUR, also commonly referred to as the uncertainty product $\mathcal{Q}(t)$. An analytic expression for $\mathcal{Q}(t)$ would allow for a better understanding of how the TUR arises in superconducting circuits. Lastly, we aim to explicitly prove the TUR for systems described by Eq. (2.16), which would provide valuable insights into the conditions under which the TUR is saturated. For practical applications, saturation mark an optimal trade-off between precision and thermodynamic cost and is therefore of special interest.

3.1 Description via First Passage Times

For a more general analysis, we first aim to express the TUR in terms of dimensionless quantities. To do so, we start by expressing Eq. (2.16) using dimensionless variables. In analogy to Sec. 2.1, define the dimensionless time $\tau = t/t_0$. Substituting into Eq. (2.16) yields a dimensionless form of the overdamped Langevin equation

$$\frac{\mathrm{d}\varphi}{\mathrm{d}\tau} = -\frac{\mathrm{d}U}{\mathrm{d}\varphi} + \sqrt{2D}\,\tilde{\xi}(\tau)\,, \tag{3.1}$$

where $D = k_\mathrm{B}T/(t_0 R I_\mathrm{c}^2)$ is the dimensionless diffusion coefficient and $\tilde{\xi}(\tau) = \sqrt{t_0}\xi(\tau t_0)$ is the dimensionless counterpart to the noise $\tilde{\xi}(t)$, see Eq. (2.16). The factor $\sqrt{t_0}$ needs to be added so that the dimensionless noise $\xi(\tau)$ again is Gaussian white noise [1]. By expressing Eq. (2.19) in terms of the dimensionless time τ, dimensionless electrical current i_0 and dimensionless diffusion coefficient D, we obtain the dimensionless form of the TUR

$$\tilde{\mathcal{Q}}(\tau) = \frac{\langle\langle\varphi^2(\tau)\rangle\rangle}{\langle\varphi(\tau)\rangle}\frac{i_0}{D} \geq 2\,, \tag{3.2}$$

where $\tilde{\mathcal{Q}}(\tau)$ is the dimensionless counterpart to the uncertainty product $\mathcal{Q}(t)$. We can now move on to the goal of this chapter, which requires that we calculate

[1] This follows from $\langle\tilde{\xi}(\tau)\tilde{\xi}(\tau')\rangle = t_0\langle\xi(\tau t_0)\xi(\tau' t_0)\rangle = t_0\delta(t_0(\tau-\tau')) = \delta(\tau-\tau'))$

the mean and variance of the phase φ. Since the driving force $f(\varphi) = -dU/d\varphi$ is L-periodic, we can decompose $\varphi(t)$ into

$$\varphi(\tau) = LN(\tau) + \theta(\tau) \tag{3.3}$$

where N counts how many net transitions the process θ has passed, and $\theta(\tau) = \varphi(\tau) \mod L$ is equal to the process φ with periodic boundary conditions at 0 and L. Note that N accounts for both forward ($Lk \to L(k+1), k \in \mathbb{Z}$) and backward transitions ($Lk \to L(k-1)$). The latter is subtracted from the former so that $N(\tau) = N^+(\tau) - N^-(\tau)$. Without loss of generality, only consider the case where $i_0 > 0$. If $i_0 < 0$, the voltage due to phase oscillations would simply be negative, and the subsequent arguments also hold after substituting $\tilde{\varphi} = -\varphi$. For practical applications of superconducting circuits, we are interested in the behavior over time scales much larger than the time t_0 on which initial conditions decay. These time scales are approximated by the long-time limit $t \sim \tau \to \infty$. In the long-time limit, both the mean and variance of the circuit's phase φ grow linearly towards infinity [15, 16, 18]. As a result, the voltage expectation approaches a constant. In the long-time limit, because of $i_0 > 0$, the number of forward transitions N^+ then exceeds the number of backward transitions N^- so that $N(\tau) \to \infty$. This has already been observed for the JJ without thermal noise in Sec. 2.1. Since θ is bounded by L, we can therefore write

$$\frac{\langle \varphi(\tau) \rangle}{\tau} \longrightarrow L \frac{\langle N(\tau) \rangle}{\tau} \tag{3.4}$$

$$\frac{\langle\langle \varphi^2(\tau) \rangle\rangle}{\tau} \longrightarrow L^2 \frac{\langle\langle N^2(\tau) \rangle\rangle}{\tau} \tag{3.5}$$

for $\tau \to \infty$. Contrary to the JJ, the phase φ does no longer increase periodically because of the noise. As a result, the time it takes for the process to go from a state $Lk \to L(k+1)$ fluctuates for different $k \in \mathbb{N}$. We denote this so-called First Passage Time (FPT) as

$$\tau\left(Lk \to L(k+1)\right) = \min\{\tau | \varphi \geq L(k+1)\} - \min\{\tau | \varphi \geq Lk\}. \tag{3.6}$$

In the long-time limit, we can express the counter N via a sum of FPTs

$$N(\tau) \approx \max\{n | S_n \leq \tau\} \quad \text{where } S_n = \sum_{k=1}^{n} \tau\left(Lk \to L(k+1)\right) \,, \tag{3.7}$$

see [8]. Note that $N(\tau) < n$ unless $S_n = \tau$, for which the latter becomes an equality. This is because $\max\{n | S_n \leq \tau\}$ does not account for the backward transitions during the time frame $(S_n, \tau]$. Since the driving force of the process is periodic and the noise is white and Gaussian, the FPTs are independent and identically distributed (i.i.d). It follows that the moments of the FPTs are independent of k, which we denote as

$$T_n\left(Lk \to L(k+1)\right) := \langle \tau\left(Lk \to L(k+1)\right)^n \rangle = T_n\left(0 \to L\right). \tag{3.8}$$

For now, assume that the mean of the FPT (also called the MFPT) and its variance are finite [2]. A finite MFPT implies that the number of backward transitions $n - N(\tau)$ during the time frame $(S_n, \tau]$ is almost surely (a.s.) finite, and therefore $N(\tau) \approx n$ in the long-time limit. Together with Eq. (3.7), it follows that

$$\frac{S_n}{N(\tau)} \leq \frac{\tau}{N(\tau)} \leq \frac{S_{n+1}}{N(\tau)+1}\left(1+\frac{1}{N(\tau)}\right) , \tag{3.9}$$

see Ref. [8]. In the long-time limit, the term in brackets approaches 1 because of $N(\tau) \to \infty$. Since the FPTs are i.i.d. with finite mean $T_1(0 \to L)$, we deduce from the strong law of large numbers that

$$T_1(0 \to L) \leq \lim_{\tau\to\infty}\left(\frac{\tau}{N(\tau)}\right) \leq T_1(0 \to L) \quad \text{a.s.} , \tag{3.10}$$

see Ref. [8]. Since the variance $\Delta T_2(0 \to L) = T_2(0 \to L) - T_1^2(0 \to L)$ is also finite (and positive), we can further invoke the Central Limit Theorem (CLT), which states that

$$\frac{S_n - nT_1(0 \to L)}{\sqrt{\Delta T_2(0 \to L)}\sqrt{n}} \xrightarrow{\text{d}} \mathcal{N}(0,1) \tag{3.11}$$

in the distributional sense, where $\mathcal{N}(0,1)$ is the normal distribution with mean 0 and variance 1. In the long-time limit, after (informally) substituting $S_n \approx \tau$ and $n \approx N(\tau)$ and using Eq. (3.10), we obtain

$$\frac{N(\tau) - \tau/T_1(0 \to L)}{\sqrt{\tau\Delta T_2(0 \to L)/T_1(0 \to L)^3}} \xrightarrow{\text{d}} \mathcal{N}(0,1). \tag{3.12}$$

This expression is referred to as the Renewal Theory CLT [8]. We thus rediscovered that the phase's fluctuations are approximately Gaussian over large time scales [12]. Together with Eq. (3.4) and Eq. (3.5), we deduce that in the long-time limit

$$\frac{\langle\varphi(\tau)\rangle}{\tau} \longrightarrow L\frac{1}{T_1(0 \to L)} \tag{3.13}$$

$$\frac{\langle\langle\varphi^2(\tau)\rangle\rangle}{\tau} \longrightarrow L^2\frac{\Delta T_2(0 \to L)}{T_1(0 \to L)^3}. \tag{3.14}$$

These relations were first derived in Ref. [16], where the authors used a similar approach. Substituting both into Eq. (3.2) allows us to express the TUR in terms of the mean and variance of the FPT

$$\tilde{\mathcal{Q}} = L\frac{\Delta T_2(0 \to L)}{T_1(0 \to L)^2}\frac{i_0}{D} \geq 2 \tag{3.15}$$

in the long-time limit. Here, $\tilde{\mathcal{Q}} = \lim_{\tau\to\infty}\tilde{\mathcal{Q}}(\tau)$ This leaves $T_1(0 \to L)$ and $\Delta T_2(0 \to L)$ to be determined, which are calculated in the next section.

[2] this is rigorously proven in the next section

3.2 Mean and Variance of the First Passage Time

The goal of this section is to calculate the mean and variance of the FPT. By doing so, we validate our previous assumption that both are finite, and thus finalize the derivation of an analytical expression for the uncertainty product $\mathcal{Q}$. For this, consider the power of the FPT $\tau(\varphi \to b)^n$ with $\varphi \leq b$, where the FPT is defined according to Eq. (3.6). Assume that the process starts at $\varphi + \Delta\varphi$. Compared to starting at φ, the time it takes for the process to reach the state b is shorter by $\Delta\tau$. It follows that

$$\begin{aligned}\tau(\varphi + \Delta\varphi \to b)^n &= (\tau(\varphi \to b) - \Delta\tau)^n \\ &\approx \tau(\varphi \to b)^n - n\tau(\varphi \to b)^{n-1}\Delta\tau \,, \end{aligned} \tag{3.16}$$

where we Taylor expanded the expression on the LHS up to first order. Taking expectations on both sides and using the notation for the moments of the FPT according to Eq. (3.8), we obtain

$$T_n(\varphi + \Delta\varphi \to b) \approx T_n(\varphi \to b) - nT_{n-1}(\varphi \to b)\Delta\tau \,. \tag{3.17}$$

Taylor expanding the left-hand side (LHS) up to second order and setting the Taylor expansion equal to the right-hand side (RHS) of Eq. (3.17) yields

$$\frac{\mathrm{d}T_n(\varphi \to b)}{\mathrm{d}\varphi}\Delta\varphi + \frac{1}{2}\frac{\mathrm{d}^2T_n(\varphi \to b)}{\mathrm{d}\varphi^2}(\Delta\varphi)^2 = -nT_{n-1}(\varphi \to b)\Delta\tau \,. \tag{3.18}$$

To calculate the powers of the phase difference $\Delta\varphi$, we derive a differential form of the overdamped Langevin equation. After (informally) multiplying Eq. (3.1) by $d\tau$ on both sides, we obtain

$$d\varphi = -\frac{\mathrm{d}U}{\mathrm{d}\varphi} + \sqrt{2D}\, dW(\tau) \,. \tag{3.19}$$

This is called the Itô form, which is a Stochastic Differential Equation (SDE) [3]. The ill-defined $\tilde{\xi}(\tau)d\tau$ is replaced with the rigorously defined Wiener increment $dW(\tau) \sim \mathcal{N}(0, d\tau)$ [4]. By substituting the finite difference $d \to \Delta$ on both sides of Eq. (3.19), it follows that

$$\Delta\varphi = -\frac{\mathrm{d}U}{\mathrm{d}\varphi}\Delta\tau + \sqrt{2D}\Delta W(\tau) \tag{3.20}$$

$$(\Delta\varphi)^2 = \left(\frac{\mathrm{d}U}{\mathrm{d}\varphi}\Delta\tau\right)^2 - 2\frac{\mathrm{d}U}{\mathrm{d}\varphi}\sqrt{2D}\Delta\tau\Delta W + 2D(\Delta W(\tau))^2. \tag{3.21}$$

[3] Because of its differential form and rigorous treatment of noise, the Itô form is especially useful for proofs and direct numerical simulations. On the other hand, the overdamped Langevin equation provides clearer physical intuition because of the explicit time derivative

[4] The Wiener increments have mean $\langle dW(\tau)\rangle = \langle\tilde{\xi}(\tau)\rangle d\tau = 0$. The variance can be calculated as

$$\langle\langle dW^2(\tau)\rangle\rangle = \int_\tau^{\tau+d\tau}\int_\tau^{\tau+d\tau} \underbrace{\langle\tilde{\xi}(\tau_1)\tilde{\xi}(\tau_2)\rangle}_{\delta(\tau_1-\tau_2)}\, d\tau_1\, d\tau_2 = \int_\tau^{\tau+d\tau} d\tau_2 = d\tau \,.$$

The Wiener increments $\Delta W(\tau)$ have mean $\langle \Delta W(\tau) \rangle = 0$. It follows for the second moment that $\langle (\Delta W(\tau))^2 \rangle = \Delta\tau$. Taking expectations yields

$$\langle \Delta\varphi \rangle = -\frac{\mathrm{d}U}{\mathrm{d}\varphi}\Delta\tau \tag{3.22}$$

$$(\Delta\varphi)^2 = 2D\Delta\tau + \mathcal{O}((\Delta\tau)^2)\ . \tag{3.23}$$

By taking expectations of both sides of Eq. (3.18) and substituting Eq. (3.22) and Eq. (3.23) while neglecting higher-order terms, we obtain the backward Kolmogorov equation (BKE) for the moments of the FPE

$$\frac{\mathrm{d}T_n(\varphi \to b)}{\mathrm{d}\varphi}\left(-\frac{\mathrm{d}U}{\mathrm{d}\varphi}\right) + D\frac{\mathrm{d}^2T_n(\varphi \to b)}{\mathrm{d}\varphi^2} = -nT_{n-1}(\varphi \to b)\ . \tag{3.24}$$

The BKE is a linear second-order ODE with variable coefficients. It requires two conditions to uniquely determine a solution, which are given by $T_n(\varphi \to b) \geq 0$, and secondly, $T_n(\varphi = b \to b) = 0$. [5]. The BKE's general solution is given by

$$T_n(\varphi \to b) = \frac{n}{D}\int_\varphi^b dx\ \exp\!\left(\frac{U(x)}{D}\right)\int_{-\infty}^x dy\ \exp\!\left(-\frac{U(y)}{D}\right)T_{n-1}(y \to b) \tag{3.25}$$

which is obtained by substituting $z(\varphi) = -dT_n(\varphi \to b)/d\varphi$ and solving the resulting first-order ODE via separation of variables [16]. With the 0-th moment $T_0(y \to b) = 1$ (because of normalization), we can now iteratively calculate the moments of the FPT: the MFPT is given by

$$T_1(0 \to L) = \frac{1}{D}\int_0^L dx\ \exp\!\left(\frac{U(x)}{D}\right)\int_{-\infty}^x dy\ \exp\!\left(-\frac{U(y)}{D}\right). \tag{3.26}$$

We prove that the MFPT is finite by showing that the integral converges for $i_0 > 0$. With $U(\varphi - Lk) = U(\varphi) + i_0Lk$ [6] and the geometric series, we can simplify the inner integral to obtain

$$\begin{aligned}
T_1(0 \to L) &= \frac{1}{D}\int_0^L dx\ \exp\!\left(\frac{U(x)}{D}\right)\sum_{k=0}^{\infty}\int_{x-L(k+1)}^{x-Lk} dy\ \exp\!\left(-\frac{U(y)}{D}\right) \\
&= \frac{1}{D}\int_0^L dx\ \exp\!\left(\frac{U(x)}{D}\right)\sum_{k=0}^{\infty}\int_{x-L}^{x} dy\ \exp\!\left(-\frac{U(y-kL)}{D}\right) \\
&= \frac{1}{D}\sum_{k=0}^{\infty}\underbrace{\exp\!\left(-\frac{i_0L}{D}\right)^k}_{<1}\int_0^L dx\ \exp\!\left(\frac{U(x)}{D}\right)\int_{x-L}^{x} dy\ \exp\!\left(-\frac{U(y)}{D}\right) \\
&= \frac{1}{D}\frac{\displaystyle\int_0^L dx\ \exp\!\left(\frac{U(x)}{D}\right)\int_{x-L}^{x} dy\ \exp\!\left(-\frac{U(y)}{D}\right)}{\displaystyle 1-\exp\!\left(-\frac{i_0L}{D}\right)}\ ,
\end{aligned} \tag{3.27}$$

[5] The first condition arises due to the fact that the time it takes to cover the distance $b - \varphi \geq 0$ is always positive. If the process starts at its target $\varphi = b$, the time is simply 0

[6] Since $P(\varphi)$ is L-periodic, therefore $U(\varphi - Lk) = -i_0(\varphi - Lk) + P(\varphi - Lk) = i_0Lk - i_0\varphi + P(\varphi) = i_0Lk + U(\varphi)$

see Ref. [16, 17]. The denominator is always greater than 0 (since $i_0 > 0$). The numerator is finite because, for a physical system, the tilted potential $U(\varphi)$ remains finite on a bounded interval. In return, the MFPT is therefore finite, which concludes the first goal of this section. For subsequent calculations, define

$$H(x) := \int_{-\infty}^{x} dy \, \exp\left(-\frac{U(y)}{D}\right) \tag{3.28}$$

$$K(x) := \int_{x}^{\infty} dy \, \exp\left(\frac{U(y)}{D}\right). \tag{3.29}$$

in analogy to Ref. [16]. These functions exhibit some interesting properties that will prove useful in later sections: again using $U(\varphi + L) = U(\varphi) - i_0 L$, we deduce that $H(x+L) = \exp(i_0 L/D) H(x)$ and $K(x+L) = \exp(-i_0 L/D) K(x)$. It follows that the terms $K'(x)H(x)$, $H'(x)K(x)$, and $K(x)H(x)$ are L-periodic. Furthermore, $H'(x)K'(x) = -1$. Expressing the MFPT in terms of $H(x)$ and the derivative $K'(x)$ allows us to derive the symmetry

$$\begin{aligned} T_1(0 \to L) &= -\frac{1}{D} \int_0^L dx \, K'(x) H(x) \\ &\overset{\text{P.I.}}{=} \underbrace{\frac{1}{D} K(x) H(x) \Big|_0^L}_{=0} + \frac{1}{D} \int_0^L H'(x) K(x) \end{aligned} \tag{3.30}$$

which becomes important for later calculations [16]. Additionally, define

$$\tilde{I}_+(x) := -\frac{1}{D} K'(x) H(x) \tag{3.31}$$

$$\tilde{I}_-(x) := \frac{1}{D} H'(x) K(x) \tag{3.32}$$

in analogy to Ref. [16]. These functions are given by

$$I_+(x) = \frac{1}{D} \exp\left(\frac{V(x)}{D}\right) \int_{x-L}^{x} dy \, \exp\left(-\frac{V(y)}{D}\right) \tag{3.33}$$

$$\tilde{I}_+(x) = \frac{1}{D} \exp\left(\frac{U(x)}{D}\right) \int_{-\infty}^{x} dy \, \exp\left(-\frac{U(y)}{D}\right) = \frac{I_+(x)}{1 - \exp\left(-\frac{i_0 L}{D}\right)} \tag{3.34}$$

$$I_-(x) = \frac{1}{D} \exp\left(-\frac{V(x)}{D}\right) \int_{x}^{x+L} dy \, \exp\left(\frac{V(y)}{D}\right) \tag{3.35}$$

$$\tilde{I}_-(x) := \frac{1}{D} \exp\left(-\frac{U(x)}{D}\right) \int_{x}^{\infty} dy \, \exp\left(\frac{U(y)}{D}\right) = \frac{I_-(x)}{1 - \exp\left(-\frac{i_0 L}{D}\right)}, \tag{3.36}$$

where the relation between $I_\pm$ and $\tilde{I}_\pm$ is derived by dividing the inner integration intervals of $\tilde{I}_\pm$ into sections of width L and then using the geometric series in analogy to earlier. The functions $I_\pm(x)$ and $\tilde{I}_\pm(x)$ are also L-periodic and strictly positive. Using these functions allows us to express the MFPT in a more compact form

$$T_1(0 \to L) = \int_0^L dx \, \tilde{I}_\pm(x). \tag{3.37}$$

Next, calculate the variance $\Delta T_2(0 \to L)$ using Eq. (3.25). It can be shown via a rather lengthy calculation [16] [7] that

$$\begin{aligned}\Delta T_2(0 \to L) &= \frac{2}{D}\int_{\varphi}^{b} dx\, \exp\left(\frac{U(x)}{D}\right)\int_{-\infty}^{x} dy\, \exp\left(-\frac{U(y)}{D}\right) T_1(y \to L) \\ &\quad - T_1(0 \to L)^2 \\ &= 2D\int_0^L dx\, \tilde{I}_{\pm}(x)\left[\tilde{I}_{\mp}(x)\right]^2 . \end{aligned} \tag{3.38}$$

From earlier, it is known that $\tilde{I}_+(x)$ is finite for $i_0 > 0$. Similarly, it can be shown that $\tilde{I}_-(x)$ is also finite by dividing the inner integration interval into sections of width L and then using the geometric series. As a result, $\Delta T_2(0 \to L)$ is also finite, confirming the assumptions from Sec. 3.1 and thus completing our derivation.

3.3 Proof of the Thermodynamic Uncertainty Relation

This section provides a complete proof of the TUR in the long-time limit. We start by substituting our expression for the mean $T_1(0 \to L)$ from Eq. (3.37) and our expression for the variance $\Delta T_2(0 \to L)$ from Eq. (3.38) into the TUR (see Eq. (3.15)) to obtain [8]

$$\tilde{\mathcal{Q}} = 2Li_0 \frac{\displaystyle\int_0^L dx\, \tilde{I}_-(x)\left[\tilde{I}_+(x)\right]^2}{\displaystyle\left(\int_0^L dx\, \tilde{I}_+(x)\right)^2} \geq 2\,. \tag{3.39}$$

Leveraging the Cauchy-Schwarz (C-S) inequality, we derive an upper bound for the denominator, and therefore a lower bound for the uncertainty product $\mathcal{Q}$: The Cauchy-Schwarz inequality states that

$$|\langle f, g\rangle|^2 \leq \langle f, f\rangle\langle g, g\rangle \tag{3.40}$$

where $\langle f, g\rangle$ is the standard inner product for real-valued functions. When choosing $f = \tilde{I}_+(\tilde{I}_-)^{1/2}$ and $g = (\tilde{I}_-)^{-1/2}$, by the C-S inequality

$$\left(\int_0^L dx\, \tilde{I}_+(x)\right)^2 \leq \int_0^L dx\, \tilde{I}_-(x)\left[\tilde{I}_+(x)\right]^2 \int_0^L dx\, \frac{1}{\tilde{I}_-(x)}. \tag{3.41}$$

Substituting into Eq. (3.39), we derive a lower bound for $\mathcal{Q}$

$$\tilde{\mathcal{Q}} \geq \frac{2Li_0}{\displaystyle\int_0^L dx\, \frac{1}{\tilde{I}_-(x)}}\,. \tag{3.42}$$

[7] Note that there are some sign, as well as notation errors in the original publication. These errors however do not change the result.

[8] Note that we could also write $\tilde{I}_+(x)\left[\tilde{I}_-(x)\right]^2$ in the numerator, and/or $\tilde{I}_-(x)$ in the denominator.

We can explicitly show that this lower bound is equal to 2 by expressing $\tilde{I}_-(x)$ in terms of the functions $H(x)$ and $K(x)$ (see Eq. (3.28) and Eq. (3.29)). According to Eq. (3.36), $\tilde{I}_-(x) = H'(x)K(x)/D$. Using $K'(x)H'(x) = -1$, we deduce that $1/\tilde{I}_-(x) = D/[H'(x)K(x)] = -DK'(x)/K(x)$. The integral over $K'(x)/K(x)$ is known, resulting in

$$\tilde{\mathcal{Q}} \geq \frac{2Li_0}{D\displaystyle\int_0^L dx\,\frac{-K'(x)}{K(x)}} = \frac{2Li_0}{D\ln\left(\dfrac{K(0)}{K(L)}\right)} = \frac{2Li_0}{D\ln(\exp(i_0L/D))} = 2\,, \tag{3.43}$$

where $K(x+L) = \exp(-i_0L/D)K(x)$ was used in the penultimate step [9]. We thus recovered the known fact that the TUR holds for overdamped systems in the long-time limit [9, 12]. We further showed that for overdamped circuits with arbitrary periodic CPRs, the TUR is equivalent to the C-S inequality. Since the C-S inequality is well understood, this opens new possibilities for further insight into the TUR and the conditions for an optimal trade-off between precision and thermodynamic cost, which is explored in the next chapter.

[9] When using $\tilde{I}_-$ instead of $\tilde{I}_+$ in the denominator in the beginning, the same result is obtained. This would then involving the function $H(x)$ instead of $K(x)$ at the end.

Chapter 4

Impact of special Current-Phase Relations

The goal of this chapter is to explore how the form of the CPR affects the uncertainty product $\tilde{\mathcal{Q}}$ in the long-time limit. For practical applications, it is desired to saturate the TUR, which corresponds to $\tilde{\mathcal{Q}} = 2$. In the first section, we derive the conditions that lead to saturation, using the analytical expression derived in the previous chapter. We further conjecture a tighter bound for the uncertainty product than the TUR. In the last two sections, we examine two important tilted periodic potentials in superconducting circuits and study how their parameters influence the uncertainty product. We further investigate the validity of our conjecture for these two systems and extract the conditions under which the conjecture fails.

4.1 Saturating the Thermodynamic Uncertainty Relation

We proved in 3.3 that the TUR is equivalent to the Cauchy-Schwarz inequality, see Eq. (3.40). The latter reduces to an equality if and only if the two functions f and g are linearly dependent [1]. As a result, the TUR is satisfied if and only if

$$\begin{aligned} \tilde{I}_+(x)\sqrt{\tilde{I}_-(x)} &= C\frac{1}{\sqrt{\tilde{I}_-(x)}} \\ \Leftrightarrow \frac{\mathrm{d}\tilde{I}_+\tilde{I}_-}{\mathrm{d}x} &= 0\,, \end{aligned} \tag{4.1}$$

[1] Strictly speaking, the functions must be linearly dependent almost everywhere. In the context of physically meaningful EPRs however it is reasonable to only consider the case of unconstrained linear dependence.

where $C \neq 0$ is a constant. To calculate the derivative term, we first calculate the individual derivatives

$$\begin{aligned}\frac{\mathrm{d}\tilde{I}_\pm}{\mathrm{d}x} &= \frac{\mathrm{d}}{\mathrm{d}x}\left(\pm\frac{1}{D}\exp\left(\pm\frac{U(x)}{D}\right)\int_{\mp\infty}^{x} dy\, \exp\left(\mp\frac{U(y)}{D}\right)\right) \\ &= \pm\frac{1}{D}\frac{\mathrm{d}U}{\mathrm{d}x}\tilde{I}_\pm(x) \pm \frac{1}{D}\,. \end{aligned} \tag{4.2}$$

Substituting the derivatives according to Eq. (4.2) into Eq. (4.1), we obtain a more concise condition for saturation,

$$\begin{aligned}\frac{\mathrm{d}\tilde{I}_+\tilde{I}_-}{\mathrm{d}x} &= \tilde{I}_+(x)\frac{\mathrm{d}\tilde{I}_-}{\mathrm{d}x} + \tilde{I}_-(x)\frac{\mathrm{d}\tilde{I}_+}{\mathrm{d}x} \\ &= -\frac{\tilde{I}_+(x)}{D}\left(\frac{\mathrm{d}U}{\mathrm{d}x}\tilde{I}_-(x)+1\right) + \frac{\tilde{I}_-(x)}{D}\left(\frac{\mathrm{d}U}{\mathrm{d}x}\tilde{I}_+(x)+1\right) \\ &= \frac{\tilde{I}_-(x)-\tilde{I}_+(x)}{D} = 0 \quad \Leftrightarrow \quad \tilde{I}_+(x) = \tilde{I}_-(x)\,. \end{aligned} \tag{4.3}$$

To gain a better physical understanding of this condition, we examine the functions $\tilde{I}_\pm$ more closely. Their derivatives are known from Eq. (4.2) and allow for deeper insight. For subsequent calculations, define the normalized functions over the interval $(0, L)$

$$\tilde{J}_\pm(x) = \frac{\tilde{I}_\pm(x)}{\displaystyle\int_0^L dx\; \tilde{I}_\pm(x)} = \frac{\tilde{I}_\pm(x)}{T_1(0\to L)} \tag{4.4}$$

in analogy to Ref. [20]. From Sec. 3.2 we know that $\tilde{I}_\pm$ are L-periodic, hence $\tilde{J}_\pm$ are also periodic. Multiplying both sides of Eq. (4.2) for the function $\tilde{I}_-$ with D, rescaling by the MFPT and substituting φ for x yields

$$\frac{1}{T_1(0\to L)} = -\frac{\mathrm{d}U(\varphi)}{\mathrm{d}\varphi}\tilde{J}_-(\varphi) - D\frac{\mathrm{d}\tilde{J}_-(\varphi)}{\mathrm{d}\varphi}\,. \tag{4.5}$$

This equation corresponds to the stationary Fokker-Planck Equation (FPE) with the driving force $-dU/d\varphi$ and periodic boundary conditions at 0 and L. The latter stems from the fact that $\tilde{J}_\pm$ are L-periodic. The general FPE describes how the Probability Density Function (PDF) of the phase φ evolves with time. It can be derived directly from the overdamped Langevin equation given by Eq. (2.16): since the phase evolution is a Markovian (memoryless) process, see Sec. 2.2, probability is conserved and therefore follows a continuity equation

$$\begin{aligned}\frac{\partial p}{\partial \tau} + \frac{\partial j}{\partial \varphi} &= 0 \\ \text{where } j(\varphi,\tau) &= -\frac{\mathrm{d}U}{\mathrm{d}\varphi}p(\varphi,\tau) - D\frac{\partial p}{\partial \varphi}\end{aligned} \tag{4.6}$$

with PDF $p(\varphi, \tau)$. The probability current j is derived by the contribution of the deterministic force $(-dU/d\varphi)p(\varphi,\tau)$ and the diffusion contribution, which

is given by Fick's law of diffusion $j_{\text{diff}} = -D\partial p/\partial\varphi$ [18]. It is well known that for a periodic deterministic force described by a tilted periodic potential, the long-time evolution of φ is equivalent to the stationary state on a circle with the stationary probability current $j = 1/T_1(0 \to L) = \langle v\rangle/L$ [5, 3]. As a result, the FPE reduces to Eq. (4.5). The function $\tilde{J}_-$ therefore corresponds to the stationary PDF of the wrapped process $\theta = \varphi \bmod L$ on a circle, which has already been featured in Eq. (3.3). In analogy, a similar expression for $\tilde{I}_+$ in terms of the function $\tilde{J}_+$ is obtained by

$$-j = \frac{\mathrm{d}U(\varphi)}{\mathrm{d}\varphi}\tilde{J}_+(\varphi) - D\frac{\mathrm{d}\tilde{J}_+(\varphi)}{\mathrm{d}\varphi} \ . \tag{4.7}$$

This equation is the FPE with the stationary PDF $\tilde{J}_+$ and the reversed drift force $-dU/d\varphi \to +dU/d\varphi$, under the condition that the magnitude of the probability current is conserved [2]. We thus obtain a physical interpretation of the reciprocal $1/\tilde{I}_\pm(\varphi) = T_1(0 \to L)/\tilde{J}_\pm(\varphi)$ as the local mean velocity of the "phase particle" in state φ: when a state on the circle is unlikely, the probability $\tilde{J}_\pm(\varphi)$ is small and therefore $\tilde{I}_\pm(\varphi)$ is large, which means that the "phase particle" quickly moves through it. The opposite is true for states with high probability $\tilde{J}_\pm(\varphi)$. Intuitively, probability tends to accumulate near local minima, and is repelled from local maxima. However, when reversing the driving force $-dU/d\varphi \to dU/d\varphi$, local minima become local maxima. As a result, this behavior is inverted, leading to a discrepancy between the stationary PDFs. For bias currents above the critical current, all local minima disappear, which reduces this discrepancy. Even though the local minima vanish in this case, any spacial variation of the drift force $-dU/d\varphi$ still leads to a discrepancy between local mean velocities under drift reversion, thus violating TUR saturation. The saturation condition $\tilde{I}_+(x) = \tilde{I}_-(x)$, which is equivalent to$\tilde{J}_+(x) = \tilde{J}_-(x)$ therefore implies that the tilted periodic potential must have $d^2U/d\varphi^2 = 0$ everywhere, which corresponds to an affine function $U(\varphi) \sim a\varphi + b$. Indeed, when adding Eq. (4.5) and Eq. (4.7) together and substituting $\tilde{J}_- = \tilde{J}_+$, we obtain

$$2D\frac{\mathrm{d}\tilde{J}_\pm}{\mathrm{d}\varphi} = 0 \Leftrightarrow \tilde{J}_+(x) = \tilde{J}_-(x) = \frac{1}{L} = \text{const} \Leftrightarrow -\frac{\mathrm{d}U}{\mathrm{d}x} = \text{const} \ . \tag{4.8}$$

This only leaves the possibility of $P = \text{const}$ and hence $dP/d\varphi = 0$. In the scope of periodic CPRs, this condition is only satisfied for circuits that behave like an Ohmic resistor for arbitrary electric currents and thermal noise strengths. Conversely, we expect the TUR to be far from saturation when the PDFs of the forward and drift-reversed processes differ significantly. This effect should be most pronounced at small currents, where the potential's local minima become most pronounced. Under these conditions, especially with low noise, probability density tends to accumulate near the local minima, amplifying the disparity between the forward and reversed process PDFs. Furthermore, the saturation condition $\tilde{J}_- = \tilde{J}_+$ implies that the uncertainty product is closely related to

[2]For antisymmetric EPRs $P(\varphi) = -P(-\varphi)$, this equation is also obtained for $\tilde{J}_-(-\varphi)$ after applying the transformation $\varphi \to -\varphi$. This implies $\tilde{I}_+(\varphi) = \tilde{I}_-(L-\varphi)$ for symmetric CPRs.

the differential resistance

$$r_{\mathrm{d}} = \frac{\mathrm{d}\langle v\rangle}{\mathrm{d}i_0} = L\int_0^L dx\, \tilde{J}_+(x)\tilde{J}_-(x)\ , \tag{4.9}$$

see [10], since is directly proportional to the scalar product $\langle \tilde{J}_+, \tilde{J}_-\rangle$. A derivation of this formula is also found in App. A. In the case of TUR saturation, the differential resistance is $r_{\mathrm{d}} = 1$. These observations suggest that when the PDFs of the forward and drift-reversed processes differ significantly, the differential resistance could deviate substantially from unity (either much smaller or much larger than 1). However, a rigorous proof of this relationship remains elusive. Although in the long-time limit, the TUR is only saturated for Ohmic behavior, we can identify three limits in which the TUR is close to saturation. For the subsequent calculations, it is more advantageous to express the TUR in terms of the functions $I_\pm$, see Eq. (3.33) and Eq. (3.35): unlike $\tilde{I}_\pm$, the functions $I_\pm$ are defined with finite integration limits, making approximations of the integrands more tractable. Substituting $I_\pm$ into the TUR, see Eq. (3.39), yields

$$\tilde{\mathcal{Q}} = \frac{2Li_0}{1-\exp\left(-\dfrac{i_0L}{D}\right)} \frac{\displaystyle\int_0^L dx\, I_\pm(x)\,[I_\mp(x)]^2}{\displaystyle\left(\int_0^L dx\, I_\pm(x)\right)^2} \geq 2\ . \tag{4.10}$$

For large currents $i_0 \gg \max\{|dP/d\varphi|\}$, the tilted periodic potential is dominated by its linear component,

$$\frac{U(x)}{D} \approx -\frac{i_0 x}{D} \tag{4.11}$$

which is an affine function, hence $\tilde{\mathcal{Q}} \approx 2$. For large noise $D \gg \max\{i_0L, |P(\varphi) - i_0\varphi|\}, \varphi \in (-L, L)$,

$$\exp\left(\pm\frac{U(x)}{D}\right) \approx 1\ , \tag{4.12}$$

such that thermal noise outweighs the deterministic relations of the circuit, and the phase's dynamics is governed purely by thermal diffusion. This indicates that $\tilde{\mathcal{Q}}$ is monotonically increasing for decreasing D, however a formal proof has not yet been developed. Substituting Eq. (4.12) into Eq. (4.10), we again obtain

$$\tilde{\mathcal{Q}} \approx \frac{2i_0L}{D\left(1-\exp\left(-\dfrac{i_0L}{D}\right)\right)} \approx 2\ , \tag{4.13}$$

where the first-order Taylor expansion of the exponential was used in the last step. This hints at a tendency that the uncertainty product is (strictly) increasing for decreasing noise D. However, such a claim has not been rigorously proven. For small currents $i_0 \ll D/L$, the circuit approaches an equilibrium steady state. The exponential is dominated by the periodic component of the

potential

$$\pm \int_{x\mp L}^{x} dy\, \exp\left(\mp \frac{U(y)}{D}\right) \approx \pm \int_{x\mp L}^{x} dy\, \exp(0) \exp\left(\mp \frac{P(y)}{D}\right) = \pm \int_{0}^{L} dy\, \exp\left(\mp \frac{P(y)}{D}\right), \tag{4.14}$$

therefore the inner integrals of $I_\pm$ are constant for all x. Substituting into Eq. (4.10) and simplifying yields the same expression as in the large noise limit, which again resulting in $\tilde{\mathcal{Q}} \approx 2$. This result is counterintuitive: for $i_0 \to 0$, the tilt is too small to smooth smooth out local minima and maxima. As a result, the stationary PDFs of the forward and drift-reversed processes accumulate in local minima, which indicates a strong violation of the saturation condition, especially for small noise. This however is not observed, as we just showed. The condition that small overlap of the PDFs implies that $\tilde{\mathcal{Q}} \gg 2$ is therefore only valid far away from equilibrium, e.g $i_0 \gtrsim D/L$. This concludes our analytical investigation of the conditions for saturation. In practice, the mean and variance of the phase are difficult to determine, which renders an estimate of the uncertainty product challenging. We conjecture the inequalities

$$\tilde{\mathcal{Q}} \geq 2\frac{r_\mathrm{d}\, i_0}{\langle v \rangle} \geq 2\,. \tag{4.15}$$

for symmetric and periodic EPRs $P(\varphi) = P(-\varphi)$. This intermediate bound of the uncertainty product features only the dimensionless variables i_0, the differential resistance r_d and the voltage expectation $\langle v \rangle$, which can be directly obtained from the I-V curve. In the context of superconducting circuits, this enables a much more tractable understanding of the TUR. The term

$$\tilde{\mathcal{L}} := 2\frac{r_\mathrm{d}\, i_0}{\langle v \rangle} = 2\left(\frac{\mathrm{d}\langle v \rangle}{\mathrm{d}i_0}\right)\left(\frac{\langle v \rangle}{i_0}\right)^{-1} \tag{4.16}$$

is a multiple of the ratio of the differential r_d and static resistance $\langle v \rangle / i_0$, which can be interpreted as a measure of nonlinearity. $\tilde{\mathcal{L}}$ is conjectured to be equal to 2 for linear systems with a symmetric EPR, and greater than 2 for nonlinear systems. The expected voltage is given by Stratonovich's formula for the velocity of a Brownian particle in the overdamped limit, which is related to the MFPT in the long-time limit via

$$\langle v \rangle = \langle \dot{\varphi} \rangle = \frac{L}{T_1(0 \to L)}\,, \tag{4.17}$$

see Ref. [16, 3, 17]. Substituting both expressions for the expected voltage and the differential resistance, we obtain

$$\tilde{\mathcal{L}} \geq 2 \Leftrightarrow i_0 \int_0^L dx\, \tilde{I}_+(x)\tilde{I}_-(x) - \int_0^L dx\, \tilde{I}_\pm(x) \geq 0 \tag{4.18}$$

for the lower bound of $\tilde{\mathcal{L}}$. For Ohmic behavior the circuit behaves linearly, therefore $\tilde{\mathcal{L}} = 2$. The same also holds in thermal equilibrium. For the upper bound of $\tilde{\mathcal{L}}$ we obtain the equivalent expression

$$\tilde{\mathcal{Q}} \geq \tilde{\mathcal{L}} \;\Leftrightarrow\; D_{\text{eff}} \geq D\, r_{\text{d}} = \mu \,. \tag{4.19}$$

The effective diffusion coefficient quantifies the speed at which the variance spreads via

$$D_{\text{eff}} = \lim_{\tau\to\infty} \frac{\langle\langle \varphi^2(\tau)\rangle\rangle}{2\tau} = DL^2 \frac{\int_0^L dx\, \tilde{I}_{\pm}(x) \left[\tilde{I}_{\mp}(x)\right]^2}{\left(\int_0^L dx\, \tilde{I}_{\pm}(x)\right)^3} \,, \tag{4.20}$$

which is derived in Ref. [16]. after some algebraic transformations [3], where μ is the mobility, which is commonly used in the context of Brownian motion. The inequality reduces to the Einstein-Smoluchowski relation $D_{\text{eff}} = D\, r_{\text{d}}$ for both Ohmic behavior as well as in equilibrium. The inequality from Eq. (4.19)was first conjectured in the year 2005 and published in Ref. [20]. It was conjectured to hold for arbitrary symmetric EPRs, and for antisymmetric EPRs under additional conditions; however, to the author's best knowledge, no additional research towards a rigorous proof has been conducted since. If proven to hold, Eq. (4.15)would not only provide a tighter bound for the uncertainty product than the TUR, but also imply a physically meaningful connection to the circuit's differential resistance, current, and voltage expectation.

4.2 Josephson Junction

We now examine the uncertainty product for the JJ with thermal noise. The analytical result from Eq. (3.39) is backed up by Monte Carlo (MC) simulations leveraging the Euler-Maruyama method [11].Additionally, we investigate the validity of our conjecture from Sec. (4.1), examining both the conjectured upper and lower bounds of $\tilde{\mathcal{L}}$. The values are plotted in Fig. 4.1. The MC results show excellent agreement with analytical predictions. Across all considered currents and diffusion coefficients, $\tilde{\mathcal{Q}}$ is strictly increasing for decreasing D. As expected, the uncertainty product exceeds the theoretical lower limit of $\tilde{\mathcal{Q}} = 2$. This confirms our analytical expectations: the JJ's EPR $P(\varphi) = -\cos(\varphi) \neq \text{const}$ and therefore does not meet the conditions for saturation as derived in Sec. 4.1. In the three regimes discussed earlier, Sec. 4.1, the TUR approaches saturation: for large noise $D \gg 2\pi i_0$, the uncertainty product indeed approaches $\tilde{\mathcal{Q}} \approx 2$, which confirms analytical predictions. The same is observed for large currents $i_0 \gg 1/(2\pi)$ and small currents $i_0 \ll D/(2\pi)$. Interestingly, the rate at which the TUR approaches saturation for small currents is much larger than for large

[3] An equivalent covariance-like condition $\text{Cov}_{\text{u}}(\tilde{I}_{-}\tilde{I}_{+}, \tilde{I}_{\pm}) \geq 0$ is also obtained via similar algebraic transformations. Here, u denotes the uniform measure over the domain $(0, L)$

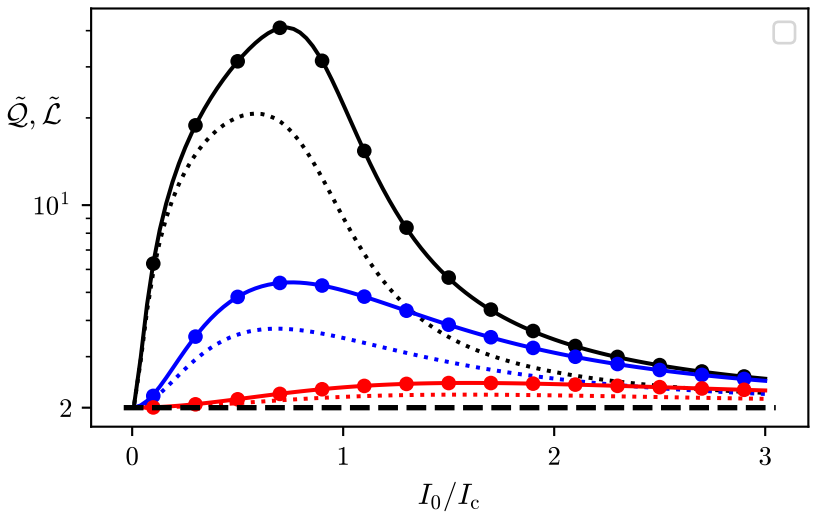

Figure 4.1: Uncertainty product $\tilde{\mathcal{Q}}$ and nonlinearity measure $\tilde{\mathcal{L}}$ for the JJ for different currents I_0 and diffusion coefficients D. Black dashed line: theoretical lower bound of 2. Solid lines: uncertainty product $\tilde{\mathcal{Q}}$ for different diffusion coefficients $D = 0.1$ (black), $D = 0.5$ (blue) and $D = 1.5$ (red). Circular markers: results for $\tilde{\mathcal{Q}}$ obtained via Monte Carlo simulations, averaged over 10^5 trajectories. The uncertainties are so small that error bars are not visible. Dotted lines: nonlinearity measure $\tilde{\mathcal{L}}$, which is the conjectured tighter lower bound of $\tilde{\mathcal{Q}}$, evaluated for the same diffusion coefficients and following the same color scheme. Inside the considered current range, the conjecture $\tilde{\mathcal{Q}} \geq \tilde{\mathcal{L}} \geq 2$ for symmetric EPRs, holds.

currents [4]. Since the conjecture from Sec. 4.1 holds across the considered current range, this observation can be explained by considering the nonlinearity measure $\tilde{\mathcal{L}}$. For small currents, the behavior of the JJ is dominated by its highly nonlinear CPR, whereas for larger currents, the linear Ohmic component $-i_0\varphi$ of the tilted periodic potential dominates. As a result, $\tilde{\mathcal{L}}$ is much larger for small currents than for large currents for a constant diffusion coefficient D. Since $\tilde{\mathcal{L}}$ bounds the uncertainty product from below, this also results in large $\tilde{\mathcal{Q}}$ for small currents. For large noise, the phase approaches free diffusion, which is linear [5], hence $\tilde{\mathcal{L}} \approx 2$. This claim is supported by our analytical results from Sec. 4.1 in the large noise limit. Fig. 4.1 also shows that for decreasing noise, $\tilde{\mathcal{Q}}$ moves away from saturation. This is explained by interpreting the saturation condition as an inversion symmetry of the stationary PDF under drift reversion, see Sec. 4.1. Consider the current $I_0 = 0.8I_c$. Since the current bias is smaller than the critical current, the local minima tend to trap the "phase particles",

[4] In log space, $\tilde{\mathcal{Q}}$ appears approximately symmetric, which corresponds to a strongly skewed distribution in linear space

[5] The drift force for free diffusion is 0. Consequently, the overdamped Langevin equation is linear.

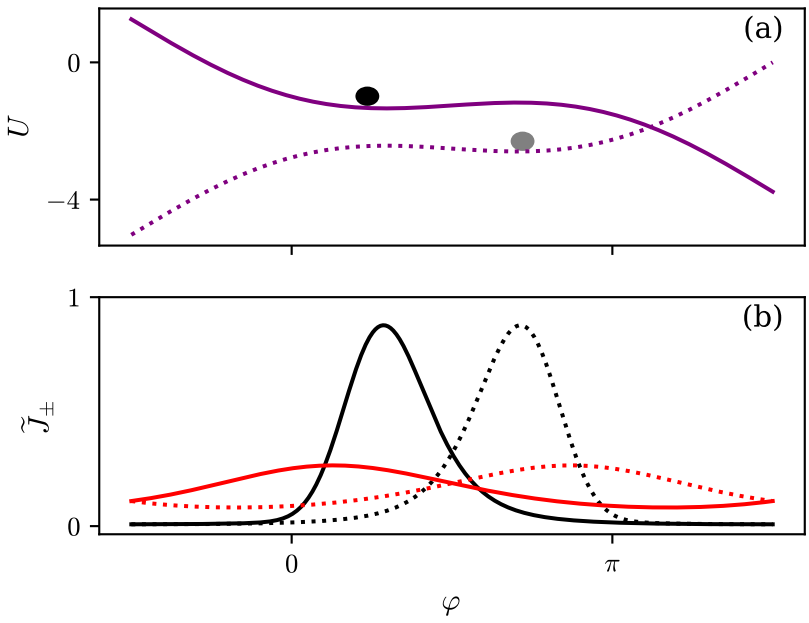

Figure 4.2: (a): tilted washboard potentials corresponding to the forward drift force $-dU/d\varphi = i_0 - \sin(\varphi)$ (solid line) with $i_0 = 0.8$, and its reverse (dotted line). The circles represent "phase particles" inside local minima, at which the PDF is large. (b): PDF $\tilde{J}_-$ of the forward process (solid lines), and PDF $\tilde{J}_+$ corresponding to the drift-reversed process (dotted lines). The PDFs are calculated for the diffusion coefficients $D = 0.1$ (black) and $D = 1.5$ (red). Far from equilibrium, a strong overlap of $\tilde{J}_\pm$ corresponds to a lower uncertainty product $\tilde{\mathcal{Q}}$ and vice versa, which is observed in Fig. 4.1.

which can only escape via thermal fluctuations. A visual figure is plotted in Fig. 4.2. Under drift reversion, the local minima become local maxima and vice versa. As a result, the forward and the drift-reversed process trap the particle at different phases. Since the accumulation of probability is smeared out by large noise D, the PDFs $\tilde{J}_\pm$ of both processes strongly overlap for large noise $D = 1.5$, whereas for small noise $D = 0.1$ they strongly differ. This indicates a strong violation of the saturation condition for $D = 0.1$, leading to $\tilde{\mathcal{Q}} >> 2$, which is indeed observed in Fig. 4.1. Contrary to intuition, $\tilde{\mathcal{Q}}$ is not maximized for the critical current $I_0 = I_c$. Instead, the location of the maximum also depends on the noise strength D. For small noise, the maximum is obtained below the critical current, whereas for large noise, it moves towards larger currents. It however remains unclear why this effect occurs.

4.3 Sawtooth Ratchet

In general, the sawtooth potential is a spatially asymmetric potential. Contrary to the JJ, it allows for non-reciprocal behavior, which means that the dynamics

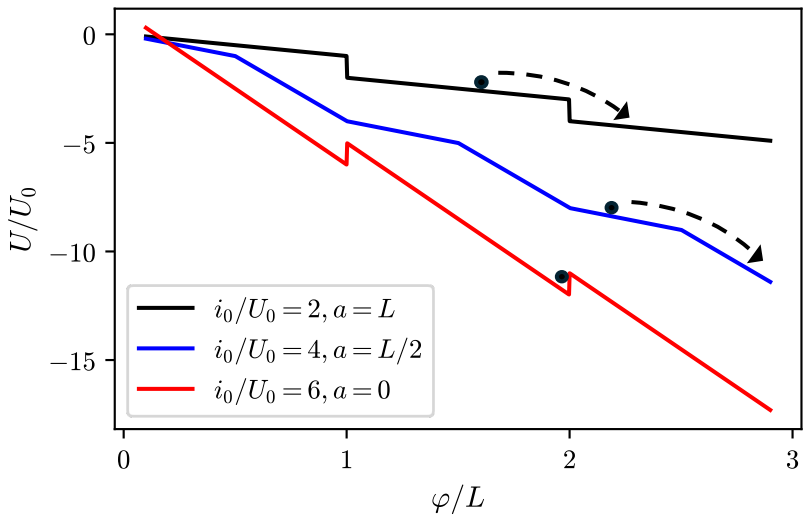

Figure 4.3: Tilted sawtooth potential for different ratios i_0/U_0 and a/L. In analogy to the JJ from Sec. 2.1, the potential exhibits local minima below a certain critical current that depends on the ratio a/L. When the tilt of the potential exceeds this critical current, all local minima disappear and the "phase particle" runs down the slope indefinitely, which results in a net voltage. For $a = 0$ however, the critical current is infinite, enabling an arbitrarily large supercurrent.

depend on the direction of the electrical current. Because of this, the sawtooth potential is of special interest when studying directional transport, such as the ratchet effect [19]. Furthermore, because of its piecewise linearity, it is often used as a low-complexity model, while maintaining key physical features of real potentials. Including the tilt $-i_0\varphi$, we define the tilted sawtooth potential as the sum of the tilt $-i_0\varphi$ and the sawtooth potential

$$U(\varphi) = -i_0\varphi + U_0 \cdot \begin{cases} \dfrac{w}{a} & w = \varphi \bmod L \in [0, a) \\ 1 - \dfrac{w-a}{b} & w = \varphi \bmod L \in [a, L) \end{cases}, \tag{4.21}$$

with the barrier height U_0 and the parameters a and b with $a + b = L$. The potential is visualized in Fig. 4.3 for different tilts and ratios a/L. For $a = b = L/2$, the sawtooth potential is symmetric. For all other values of a, the sawtooth potential is asymmetric, reaching its highest degree of non-reciprocity for $a = 0$ and $a = L$ for which it is antisymmetric. Setting $a = L$ is equivalent to $a = 0$ while reversing the current i_0 and vice versa. However, despite this equivalence, reversing the current in either case leads to qualitatively different circuit behavior, due to the broken spatial symmetry of the potential. In analogy to the JJ from Sec. 2.1, the potential exhibits local minima below a certain critical current that depends on the ratio a/L. When the tilt of the potential exceeds this critical current, all local minima disappear and the "phase particle" runs

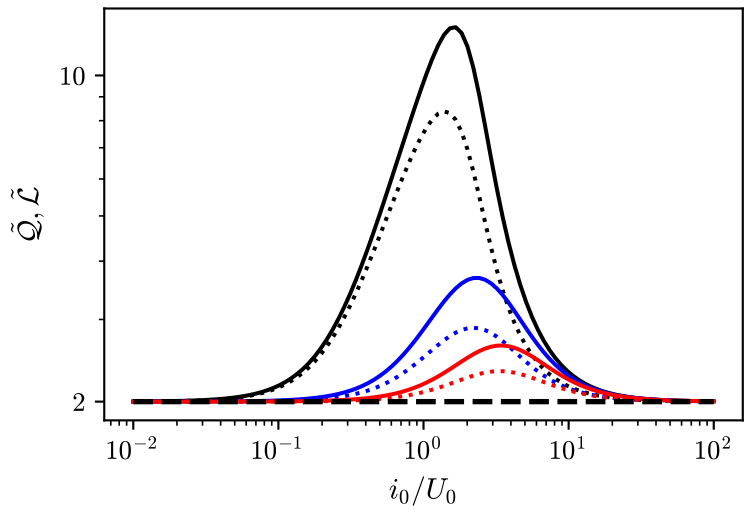

Figure 4.4: Uncertainty product $\tilde{\mathcal{Q}}$ and nonlinearity measure $\tilde{\mathcal{L}}$ for the tilted sawtooth potential for different current-to-barrier height ratios i_0/U_0 and noise-to-barrier height ratios D/U_0. The sawtooth potential is symmetric with $a = b = L/2$ and $L = 1$. Black dashed line: theoretical lower bound of 2. Solid lines: uncertainty product $\tilde{\mathcal{Q}}$ for $D/U_0 = 0.1$ (black), $D/U_0 = 0.3$ (blue) and $D/U_0 = 0.5$ (red). Dotted lines: nonlinearity measure $\tilde{\mathcal{L}}$, evaluated for the same noise-to-barrier height ratios and following the same color scheme. In the considered current range, the conjecture $\tilde{\mathcal{Q}} \geq \tilde{\mathcal{L}} \geq 2$ holds.

down the slope indefinitely, which results in a net voltage. For $a = 0$ however, the critical current is infinite, which implies that the corresponding CPR theoretically enables the transmission of an arbitrarily large supercurrent. When reversing the current i_0, the dynamics are equivalent to $a = L$, which has finite critical current as seen in Fig. 4.3. This resembles the behavior of an ideal diode, enabling a supercurrent in only one direction while blocking it in the other direction. Ref. [4] demonstrated that building a near-ideal superconducting diode is possible by combining JJs together via Fourier engineering. The tilted sawtooth potential is among the very few for which we are able to analytically solve the integrals in $T_1(0 \to L)$, $\Delta T_2(0 \to L)$ and r_d for a circuit operating in the overdamped limit. The rather lengthy step-by-step calculation for $I_\pm(x)$ is found in App. B. Since the expressions for $I_\pm$ remain complicated even in the special cases $a =$, $a = L$ or $a = b = L/2$, we refrain from computing $\tilde{\mathcal{Q}}$ and $\tilde{\mathcal{L}}$ analytically, as this would offer little analytical insight. Instead, the values for $\tilde{\mathcal{Q}}$ and $\tilde{\mathcal{L}}$ are purely calculated via numerical integration. When studying the tilted sawtooth potential in the context of the TUR, the cases $a = b = L/2$, $a = 0$ and $a = L$ are of special interest. In the first case, the sawtooth potential is symmetric. If true, we expect the conjecture $\tilde{\mathcal{Q}} \geq \tilde{\mathcal{L}} \geq 2$ to hold in this case. The two other parameterizations $a = 0$ and $a = L$ correspond to an antisymmetric tilted periodic potential, for which the conjecture is possibly

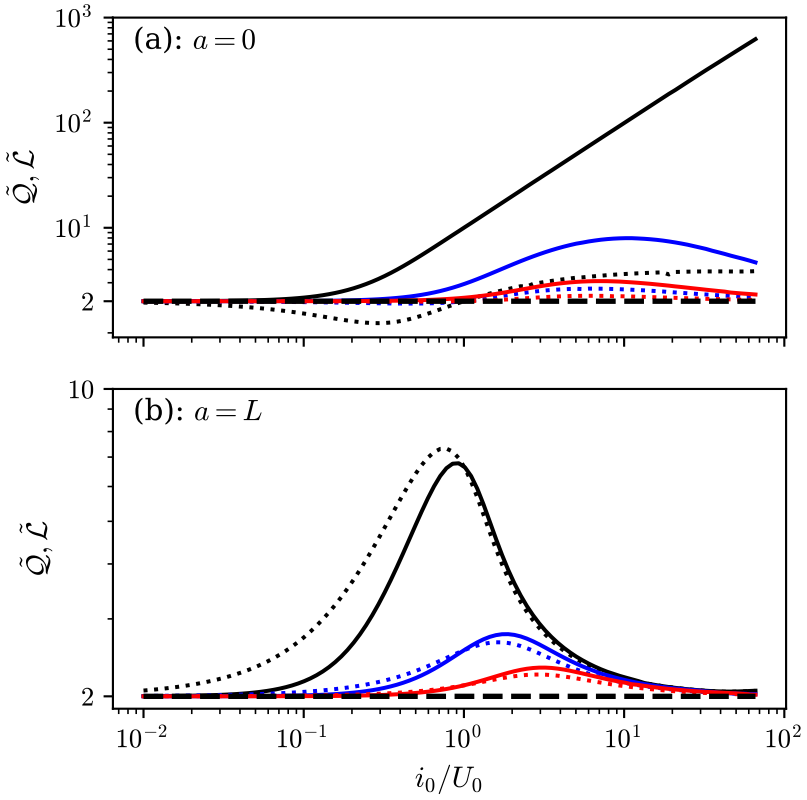

Figure 4.5: Uncertainty product $\tilde{\mathcal{Q}}$ and nonlinearity measure $\tilde{\mathcal{L}}$ for the tilted sawtooth potential for $L = 1$ and different current-to-barrier height ratios i_0/U_0 and noise-to-barrier height ratios D/U_0. (a): $a = 0$; (b): $a = L$. Exemplary plots of the potential for both parameterizations are found in Fig. 4.3. Black dashed line: theoretical lower bound of 2. Solid lines: uncertainty product $\tilde{\mathcal{Q}}$ for $D/U_0 = 0.1$ (black), $D/U_0 = 0.3$ (blue) and $D/U_0 = 0.5$ (red). Dotted lines: nonlinearity measure $\tilde{\mathcal{L}}$, which is the conjectured tighter lower bound of $\tilde{\mathcal{Q}}$, evaluated for the same noise-to-barrier height ratios and following the same color scheme. For $a = 0$, see (a), the conjectured lower bound $\tilde{\mathcal{L}} \geq 2$ is violated, while the upper bound $\tilde{\mathcal{Q}} \geq \tilde{\mathcal{L}}$ holds. The opposite is observed for $a = L$, see (b). A violation is expected, as the sawtooth potential is asymmetric in both cases, thus violating the conditions of the conjecture.

violated. The case $a = 0$ is of particular interest because the local minima at $\varphi \bmod L = 0$ persist even for arbitrarily large current-to-barrier height ratios i_0/U_0. Since probability tends to accumulate at local minima, the stationary PDF is expected to exhibit a sharp spike at $\varphi \bmod L = \epsilon \to 0^+$ just before the potential's discontinuous jump. Due to thermal noise, this spike is smeared out towards the region in front of the jump. Conversely, since the sawtooth potential's is antisymmetric, the PDF of the process under reversed driving instead spikes at $\varphi \bmod L = -\epsilon \to 0^-$. Because the voltage arises purely from noise,

the PDFs of the forward and reversed processes concentrate at different points with minimal overlap, especially for small noise intensity D. This indicates a very strong violation of the saturation condition. For the case $a = b = L/2$, the values for the uncertainty product $\tilde{\mathcal{Q}}$ and the nonlinearity measure $\tilde{\mathcal{L}}$ are shown in Fig. 4.4 for the noise-to-barrier height ratios $D/U_0 = 0.1, 0.3$ and 0.5 and for different current-to-barrier height ratios i_0/U_0. As already observed for the JJ in Sec. 4.2, decreasing the noise strength D leads to an increase in the uncertainty product across all currents i_0. Analogously to the JJ, we observe the three limits for small currents, large currents, and large noise in which the TUR approaches saturation. Contrary to intuition, the maximum of $\tilde{\mathcal{Q}}$ is not reached for $i_0/U_0 = 1$. Instead, for large noise it lies at $i_0/U_0 < 1$ and moves towards smaller i_0/U_0 when decreasing noise. The same effect is also observed for the JJ, see Sec. 4.2. The rate at which the TUR approaches saturation for small currents is much larger than for large currents [6], which is also observed for the JJ. Since the conjecture appears to hold here, this observation can be explained by considering the nonlinearity measure $\tilde{\mathcal{L}}$, in analogy to Sec. 4.2: For large currents, the linear component $U(\varphi) \approx -i\varphi$ dominates, whereas for small currents, the dynamics are governed by the nonlinear periodic component $U(\varphi) \approx P(\varphi)$. For large noise, the phase approaches free diffusion, which is also linear, hence also $\tilde{\mathcal{L}} \approx 2$. All the observations for $\tilde{\mathcal{Q}}$ in the symmetric case are also observed for $a = L$. This behavior is expected, since the tilted sawtooth potential with $a = L$ and $i_0 > 0$ exhibits similar properties as the symmetric configuration. A major difference however is that the EPR is antisymmetric. As a result, the conjecture does not hold, which is observed in Fig. 4.5. The lower bound $\tilde{\mathcal{L}} \geq 2$ still holds, while the upper bound $\tilde{\mathcal{Q}} \geq \tilde{\mathcal{L}}$ is broken. The latter implies that in the corresponding current range, the Einstein-Smoluchowski relation underestimates the speed at which the phase's variance spreads. For $a = 0$, the discontinuities in the sawtooth potential suppress noise-induced drift toward smaller values of φ, causing the variance to spread primarily in the positive direction. However, since thermal noise is unbiased, this results in an asymmetric suppression of phase fluctuations, leading to a slower overall growth of variance. This mechanism extends to general antisymmetric EPRs, which inherently suppress fluctuations in a direction-dependent manner. Such non-reciprocal behavior may help explain why the conjectured upper bound fails in these cases. The opposite is observed for the case $a = 0$, where the upper bound of the conjecture holds, while the lower bound $\tilde{\mathcal{L}}$ is violated, see Fig. 4.5. his observation implies that, within the corresponding current range, the differential resistance exhibits sublinear growth. Consequently, increasing the current bias i_0 yields only a limited increase in the expected voltage $\langle v \rangle$, suggesting that the local minima impose a strong confining effect on the phase dynamics. When examining the PDF, this is confirmed in Fig. 4.6. In (b), the stationary PDF of the forward process on the circle (black solid line) and the drift-reversed process (red dotted line) is shown for the noise-to-barrier height ratio $D/U_0 = 0.1$. As expected, almost all probability accumulates inside the

[6] In log space, $\tilde{\mathcal{Q}}$ appears approximately symmetric, which corresponds to a strongly skewed distribution in linear space

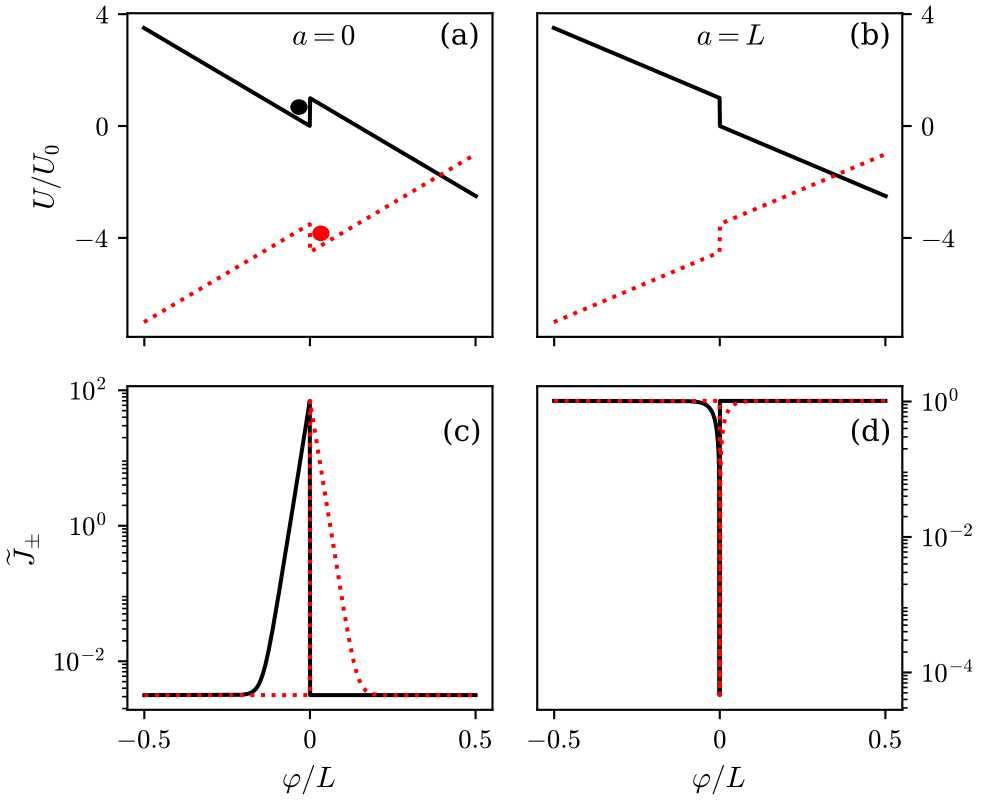

Figure 4.6: (a): tilted sawtooth potential for $L = 1$ and $a = 0$ for the noise-to-barrier height ratio $D/U_0 = 0.1$ and the current-to-barrier height ratios $i_0/U_0 = 6$ (black), and $i_0/U_0 = -6$ (red dotted). The circles represent trapped "phase particles" in local minima. (b): the same as (a) for $a = L$. (c): in black: PDF $\tilde{J}_-$ of the forward process described by the potential given by the black line in (a). in red: PDF $\tilde{J}_+$ of the drift-reversed process described by the potential given by the red line in (a). The PDFs concentrate at $\pm\epsilon$ with minimal overlap, resulting in a strong violation of the saturation condition $\tilde{I}_+(\varphi) = \tilde{I}_-(\varphi)$. (d): the same as in (c) for the forward and drift-reversed processes given by the potentials in (b). Here, most of the probability distribution remains nearly unchanged under drift reversal. Where the PDF does differ, the probability is low, indicating that the saturation condition is almost satisfied.

local minima, directly in front of the discrete jumps [7]. In the forward process, the "phase particle" is deterministically trapped inside the minimum at 0^-. In the drift-reversed process, the minimum at 0^+ traps the particle. Since the escape is purely noise-driven, probability strongly accumulates, once at 0^- and once at 0^+. As a result, this leads to a very strong violation of the TUR's satu-

[7] Here, "in front" refers to the direction in which the "phase particle" travels deterministically.

ration condition [8], which is confirmed in Fig. 4.5: compared to the JJ and the other two cases of the sawtooth potential, the uncertainty product is larger by up to 2 orders of magnitude inside the considered current range. Furthermore, the TUR approaches saturation much slower for large currents. This can be explained by the fact that for the case $a = 0$, the critical current is infinite. However, the TUR still approaches saturation as the process approaches thermal equilibrium. This is consistent with our earlier calculations from Sec. 4.1, which only required the condition $i_0 \ll D/L$. Out of the three examined cases, the TUR is closest to saturation for the case $a = 0$ across the entire current range, see Fig. 4.5. This is attributed to two characteristics: firstly, the critical current $i_0^c = U_0$ is finite. Contrary to the case $a = 0$, all local minima therefore vanish above a finite threshold. Secondly, the tilted sawtooth potential is affine across all phases except for $\varphi \bmod L = \{0^-, 0^+\}$ [9]. As a result, the PDFs of the forward and the drift-reversed process are equally constant almost everywhere, see Fig. 4.6. The only discrepancy between the two arises at $0^{\pm}$. However, since the probability is low at these points, the discrepancy between the two is minimal, implying a value for $\tilde{\mathcal{Q}}$ close to saturation.

[8] This argument holds here because $i_0/U_0 \gg D/U_0$. If this condition were not satisfied, the proximity to equilibrium would invalidate this argument.

[9] This distinguishes the case $a = L$ from the symmetric case $a = b = L/2$, for which the points where affinity is violated are spread out to $\varphi \bmod L = \{0, L/2\}$. As a result, the noise smears out a larger range of the PDF, which results in a larger discrepancy between $\tilde{J}_+$ and $\tilde{J}_-$.

Chapter 5

Conclusion and Outlook

This thesis investigated the thermodynamic uncertainty relation in superconducting circuits with a periodic current-phase relation, described by an overdamped Langevin equation with a tilted periodic potential. In Ch. 2 we analyzed the Josephson junction in the overdamped limit. We related the JJ's voltage fluctuations to a "phase particle" in the tilted periodic potential $-(I_0/I_c)\varphi - \cos(\varphi)$, described as the sum of an Ohmic term and the junction's EPR. From this analogy, we derived that the zero-voltage state of the JJ corresponds to a state in which the "phase particle" is trapped in a local minimum via the relation $V(t) \sim d\varphi/dt$. If the external current I_0 exceeds the critical current I_c, all local minima disappear and the junction enters a resistive state. This however changes when accounting for thermal noise: even when trapped, thermal fluctuations can push the "phase particle" out of the minimum, resulting in a noise-induced voltage. We quantified the precision of the integrated voltage via the square of the coefficient of variation. In the overdamped limit, the thermodynamic uncertainty relation states that increasing precision requires a thermodynamic cost in the form of a higher total entropy production. This trade-off is summarized by the uncertainty product $\tilde{\mathcal{Q}} \geq 2$, which is described in Sec. 2.3.

In Sec. 3.1 and Sec. 3.2, we derived a dimensionless expression for the TUR and analytically calculated the uncertainty product $\tilde{\mathcal{Q}}$ for the phase in the long-time limit $t \to \infty$. For this, we expressed the long-time evolution of the phase in terms of First Passage Times (FPTs). At the end of Sec. 3.1 we then used a special form of the central limit theorem to obtain the mean $\langle\varphi\rangle$ and variance $\langle\langle\varphi^2\rangle\rangle$, expressed in terms of the mean and variance of the FPT. We then derived the backward Kolmogorov equation in Sec. 3.2, from which we obtained the moments of the FPT. This concluded our derivation of an analytical expression for $\tilde{\mathcal{Q}}$. Leveraging our newly gained analytical understanding of the uncertainty product, we were able to show that the TUR is equivalent to the Cauchy-Schwarz (C-S) inequality.

In Ch. 4 we took a closer look at the saturation condition. From the equivalence of the TUR and the C-S inequality, we derived that the TUR is saturated for

all currents i_0 and noise strengths D if and only if the special functions $\tilde{I}_\pm$ are equal everywhere. In Sec. 4.1, we successfully derived a physical interpretation of this condition: the stationary PDFs of the forward process on a circle, and the process under reversed driving must be equal everywhere. This condition is only fulfilled by circuits that behave like an Ohmic resistor across all current and noise ranges. However, we also successfully identified three limits in which the TUR almost reaches saturation: for large noise, in which the process approaches free diffusion; for large currents, in which the Ohmic component dominates; and for small currents, in which the circuit approaches thermal equilibrium. At the end of Sec. 4.1, we conjectured a tighter bound than the TUR for symmetric EPRs under parity inversion, formulated in terms accessible via the I-V curve of the system. To study the influence of different EPRs on the uncertainty product and to investigate the validity of our conjecture, we then proceeded to examine $\tilde{\mathcal{Q}}$ and $\tilde{\mathcal{L}}$ for specific potentials. We chose the JJ because of its significance in superconducting circuits, and the sawtooth potential because of its simplicity and non-reciprocal properties. For the JJ, our analytical results are supported with remarkable accuracy by results obtained from Monte Carlo simulations. Our conjecture holds for the JJ, which has a symmetric EPR. In Sec. 4.3, we examined TUR for the tilted sawtooth potential. In the symmetric case as well as the antisymmetric case where $a = L$, $\tilde{\mathcal{Q}}$ closely resembles that of the JJ. However in the asymmetric case $a = 0$, the uncertainty product is several orders of magnitude larger than in the other configurations. This behavior was explained by the fact that in the case $a = 0$, the tilted sawtooth potential retains local minima for arbitrarily large currents. Furthermore, since the sawtooth potential for this case is antisymmetric under parity inversion, we observed that probability accumulates inside local minima in an antisymmetric manner under drift-reversion. We observed that this leads to a strong discrepancy between the PDFs, which leads to a strong violation of the saturation condition.

The thermodynamic uncertainty relation (TUR) provides a powerful framework for circuit design by capturing the fundamental trade-off between precision and thermodynamic cost. It enables an a priori estimate of current or voltage fluctuations based on the entropy production rate, or vice versa. A central result of this thesis is that TUR saturation across all current ranges only occurs for Ohmic systems. Another important result is that the TUR is approaches saturation in three cases: for large thermal noise, large external currents, and close to thermal equilibrium. However, when designing circuits where the trade-off between precision and entropy production is critical, the derived saturation condition often conflicts with practical requirements of superconducting circuits, which typically rely on nonlinearities. Recent studies however have shown that the TUR can be violated in underdamped systems, such as a pendulum clock [21]. This opens new possibilities for designing superconducting circuits that go beyond the theoretical limits imposed by the TUR on overdamped dynamics. It also raises the question of whether our analytical results can be extended to underdamped regimes. In both case studies involving symmetric EPRs, our conjectured tighter bound was satisfied. If proven, this bound would offer a

more practical estimate of the uncertainty product, based on quantities directly accessible from the I-V curve. Moreover, it would establish a direct link between a circuit's nonlinearity and its uncertainty product. Our conjecture further connects the uncertainty product to the differential resistance, which is proportional to the scalar product of the probability densities of the forward and drift-reversed processes–a quantity closely related to TUR saturation. This connection warrants further investigation, as it may offer a direct measure of the discrepancy between these distributions and, consequently, of the distance from saturation.

Appendix A

Differential Resistance Calculation Details

We can calculate the differential resistance using

$$r_{\mathrm{d}} = \frac{\mathrm{d}\langle v\rangle}{\mathrm{d}i_0} = \frac{\mathrm{d}}{\mathrm{d}i_0}\left(\frac{L}{T_1(0\to L)}\right) = -\frac{L}{T_1^2(0\to L)}\frac{\mathrm{d}T_1(0\to L)}{\mathrm{d}i_0}$$

The derivative of the exponential of the tilted periodic potential is

$$\frac{\mathrm{d}\exp(\pm U(\varphi)/D)}{\mathrm{d}i_0} = \mp\varphi/D\cdot\exp(\pm U(\varphi)/D)\ .$$

Substituting back yields

$$\begin{aligned}\frac{\mathrm{d}T_1(0\to L)}{\mathrm{d}i_0} &= \frac{\mathrm{d}}{\mathrm{d}i_0}\left(\frac{1}{D}\int_0^L dx\ \left[\exp\left(\frac{U(x)}{D}\right)\int_{-\infty}^x dy\ \exp\left(-\frac{U(y)}{D}\right)\right]\right)\\ &= \frac{1}{D^2}\left(\int_0^L dx\ \left[-x\exp\left(\frac{U(x)}{D}\right)\int_{-\infty}^x dy\ \exp\left(-\frac{U(y)}{D}\right)\right]\right.\\ &\qquad\left.+\int_0^L dx\ \left[\exp\left(\frac{U(x)}{D}\right)\int_{-\infty}^x dy\, y\exp\left(-\frac{U(y)}{D}\right)\right]\right)\ .\end{aligned}$$

Given an integral of this shape, one can perform partial integration

$$\begin{aligned}\int_a^b dx\, x f(x) &= \left(x\int_a^x dx'\, f(x')\right)\Big|_a^b - \int_a^b dx\ \int_a^x dx'\, f(x')\\ &= b\int_a^b dx'\, f(x') - \int_a^b dx\ \int_a^x dx'\, f(x')\ .\end{aligned}$$

Calculate the second integral using partial integration

$$\begin{aligned}&\int_{-\infty}^x dy\, y\exp\left(-\frac{U(y)}{D}\right)\\ &= x\int_{-\infty}^x dy\ \exp\left(-\frac{V(y)}{D}\right)dy - \int_{-\infty}^x dz\ \left(\int_{-\infty}^z dy\ \exp\left(-\frac{U(y)}{D}\right)\right)\end{aligned}$$

and substitute back, which yields

$$\begin{aligned}
\frac{\mathrm{d}T_1(0\to L)}{\mathrm{d}i_0} &= \frac{1}{D^2}\left(\int_0^L dx\,\left[-x\exp\!\left(\frac{U(x)}{D}\right)\int_{-\infty}^{x} dy\,\exp\!\left(-\frac{U(y)}{D}\right)\right]\right.\\
&\quad\left.+\int_0^L dx\,\exp\!\left(\frac{U(x)}{D}\right)\left[x\int_{-\infty}^{x} dy\,\exp\!\left(-\frac{U(y)}{D}\right)-\int_{-\infty}^{x} dz\,\left(\int_{-\infty}^{z} dy\,\exp\!\left(-\frac{U(y)}{D}\right)\right)\right]\right)\\
&= -\frac{1}{D^2}\int_0^L dx\,\exp\!\left(\frac{U(x)}{D}\right)\int_{-\infty}^{x} dz\int_{-\infty}^{z} dy\,\exp\!\left(-\frac{U(y)}{D}\right)\\
&= -\frac{1}{D}\int_0^L dx\,\exp\!\left(\frac{U(x)}{D}\right)\int_{-\infty}^{x} dz\,\exp\!\left(-\frac{U(z)}{D}\right)\underbrace{\frac{1}{D}\exp\!\left(\frac{U(z)}{D}\right)\int_{-\infty}^{z} dy\,\exp\!\left(-\frac{U(y)}{D}\right)}_{=\tilde{I}_+(z)}\\
&= -\frac{1}{D}\int_0^L dx\,\exp\!\left(\frac{U(x)}{D}\right)\int_{-\infty}^{x} dz\,\exp\!\left(-\frac{U(z)}{D}\right)\tilde{I}_+(z)\\
&= -\frac{1}{D}\frac{1}{1-\exp\!\left(-\frac{i_0 L}{D}\right)}\int_0^L dx\,\exp\!\left(\frac{U(x)}{D}\right)\int_{x-L}^{x} dz\,\exp\!\left(-\frac{U(z)}{D}\right)\tilde{I}_+(z)
\end{aligned}$$

The order of integration is interchangeable because of periodicity, which yields

$$\begin{aligned}
&= -\frac{1}{1-\exp\!\left(-\frac{i_0 L}{D}\right)}\int_0^L dz\,\tilde{I}_+(z)\underbrace{\frac{1}{D}\exp\!\left(-\frac{U(z)}{D}\right)\int_{x}^{x+L} dx\,\exp\!\left(\frac{U(x)}{D}\right)}_{I_-(z)}\\
&= -\int_0^L dz\,\tilde{I}_+(z)\tilde{I}_-(z)\,.
\end{aligned}$$

In total, the differential resistance simplifies to

$$r_\mathrm{d} = \frac{\mathrm{d}\overline{\langle\dot{\varphi}\rangle}}{\mathrm{d}i_0} = \frac{L}{T_1^2(0\to L)}\int_0^L dx\,\tilde{I}_+(x)\tilde{I}_-(x) = L\int_0^L dx\,\tilde{J}_+(x)\tilde{J}_-(x)\,,$$

which is the same expression as obtained in [10].

Appendix B

Sawtooth Ratchet Calculation Details

For a more compact expression, define the tilted sawtooth potential as

$$U(x) = \begin{cases} U_{\mathrm{a}}(x) = -i_0 x + U_0 \dfrac{w}{a} & w = x \bmod L \in [0, a) \\ U_{\mathrm{b}}(x) = -i_0 x + U_0 \left(1 - \dfrac{w-a}{b}\right) & w = x \bmod L \in [a, L) \end{cases}$$

with $a + b = L$, $a, b \geq 0$. Evaluate the inner integrals of the functions $I_{\pm}(x)$. Focus on evaluating the integral. Shift the integral bounds to $0, L$:

$$\int_{x-L}^{x} dy \, \exp\left(-\frac{U(y)}{D}\right) = \int_{0}^{L} dz \, \exp\left(-\frac{U(x-z)}{D}\right)$$
$$\int_{x}^{x+L} dy \, \exp\left(\frac{U(y)}{D}\right) = \exp\left(-\frac{i_0 L}{D}\right) \int_{x-L}^{x} dy \, \exp\left(\frac{U(y)}{D}\right) = \exp\left(-\frac{i_0 L}{D}\right) \int_{0}^{L} dz \, \exp\left(\frac{U(x-z)}{D}\right)$$

Evaluate the term $U(x-z)$ with $z \in [0, L]$

$$U(x-z) = \begin{cases} U_{\mathrm{a}}(x-z) = -i_0 (x-z) + U_0 \dfrac{w}{a} & w = (x-z) \bmod L \in [0, a) \quad \text{(Case a)} \\ U_{\mathrm{b}}(x-z) = -i_0 (x-z) + U_0 \left(1 - \dfrac{w-a}{b}\right) & w = (x-z) \bmod L \in [a, L) \quad \text{(Case b)} \end{cases}$$

$w = (x-z) \bmod L$ can also be written as:

$$w = (x-z) \bmod L = \begin{cases} w = x - z & \text{if } x - z \geq 0 \quad \text{(Case 1)} \\ w = x - z + L & \text{if } x - z < 0 \quad \text{(Case 2)} \end{cases}$$

The indefinite integrals are

$$\int dz\, \exp\left(\mp\frac{U(x-z)}{D}\right)\Bigg|_{(x-z)\geq 0}$$

$$= \begin{cases} \exp\left(\mp\frac{1}{D}\left(-i_0 x + U_0\frac{x}{a}\right)\right)\int dz\, \exp\left(\mp\frac{1}{D}\left(i_0 z - U_0\frac{z}{a}\right)\right) & (x-z) \bmod L \in [0,a) \\ \exp\left(\mp\frac{1}{D}\left(-i_0 x + U_0\left(1-\frac{x-a}{b}\right)\right)\right)\int dz\, \exp\left(\mp\frac{1}{D}\left(i_0 z + U_0\frac{z}{b}\right)\right) & (x-z) \bmod L \in [a,L) \end{cases}$$

$$= \begin{cases} \exp\left(\mp\frac{x}{D}\left(i_0 - \frac{U_0}{a}\right)\right)\int dz\, \exp\left(\mp\frac{z}{D}\left(i_0 - \frac{U_0}{a}\right)\right) & (x-z) \bmod L \in [0,a) \\ \exp\left(\pm\frac{1}{D}\left(i_0 x - U_0\left(1-\frac{x-a}{b}\right)\right)\right)\int dz\, \exp\left(\mp\frac{z}{D}\left(i_0 + \frac{U_0}{b}\right)\right) & (x-z) \bmod L \in [a,L) \end{cases}$$

$$= \begin{cases} \exp\left(\pm\frac{x}{D}\left(i_0 - \frac{U_0}{a}\right)\right)\left[\frac{\exp\left(\mp\frac{z}{D}\left(i_0 - \frac{U_0}{a}\right)\right)}{\mp\frac{1}{D}\left(i_0 - \frac{U_0}{a}\right)}\right]\Bigg|_z & (x-z) \bmod L \in [0, \\ \exp\left(\pm\frac{x}{D}\left(i_0 + \frac{U_0}{b}\right)\right)\exp\left(\mp\frac{U_0}{D}\left(1+\frac{a}{b}\right)\right)\left[\frac{\exp\left(\mp\frac{z}{D}\left(i_0 + \frac{U_0}{b}\right)\right)}{\mp\frac{1}{D}\left(i_0 + \frac{U_0}{b}\right)}\right]\Bigg|_z & (x-z) \bmod L \in [a, \end{cases}$$

In case of $x - z < 0$, the integral is multiplied by

$$\begin{cases} \exp\left(\mp\frac{1}{D}\frac{U_0 L}{a}\right) & (x-z) \bmod L \in [0,a] \\ \exp\left(\pm\frac{1}{D}\frac{U_0 L}{b}\right) & (x-z) \bmod L \in (a,L) \end{cases}$$

define

$$\begin{aligned} \tilde{U}_{\mathrm{a}}(x) = -U_{\mathrm{a}}(x) &= x\left(i_0 - \frac{U_0}{a}\right) \\ \tilde{U}_{\mathrm{b}}(x) &= x\left(i_0 + \frac{U_0}{b}\right) \\ \Rightarrow U_{\mathrm{b}}(x) &= -\tilde{U}_{\mathrm{b}}(x) + U_0\left(1+\frac{a}{b}\right) \\ \Rightarrow \tilde{U}_{\mathrm{b}}(x) - \tilde{U}_{\mathrm{a}}(x) &= U_0 x\left(\frac{1}{a}+\frac{1}{b}\right) \end{aligned}$$

Note that both $\tilde{U}_{\mathrm{a}}(x)$ and $\tilde{U}_{\mathrm{b}}(x)$ are linear. Further define

$$E_{\pm}^{\mathrm{a,b}}(x) = \exp\left(\pm\frac{U_{\mathrm{a,b}}(x)}{D}\right).$$

Because of the linearity of $U_{\mathrm{a}}(x)$ and $U_{\mathrm{b}}(x)$, these functions have the properties

$$\begin{aligned} E_{\pm}^{\mathrm{a,b}}(x)E_{\pm}^{\mathrm{a,b}}(y) &= E_{\pm}^{\mathrm{a,b}}(x+y) \\ E_{\pm}^{\mathrm{a,b}}(x)E_{\mp}^{\mathrm{a,b}}(y) &= E_{\pm}^{\mathrm{a,b}}(x-y) \end{aligned}$$

and in particular $E_{\pm}^{\mathrm{a,b}}(0) = 1$. Their integrals are

$$\int dx\, E_{\pm}^{\mathrm{a,b}}(\lambda x) = \pm D \frac{E_{\pm}^{\mathrm{a,b}}(\lambda x)}{\tilde{U}_{\mathrm{a,b}}(\lambda)} \ .$$

Using these definitions, the integral can then be expressed in a more compact form:

$$\begin{aligned}
&\int dz\, \exp\left(\mp \frac{U(z)}{D}\right) \\
&= \mp \begin{cases} D E_{\pm}^{\mathrm{a}}(x)) \left[\frac{E_{\mp}^{\mathrm{a}}(z)}{\tilde{U}_{\mathrm{a}}(1)}\right]\Big|_z & (x-z) \bmod L \in [0,a) \\ D E_{\pm}^{\mathrm{b}}(x)) \exp\left(\mp \frac{U_0}{D}\left(1+\frac{a}{b}\right)\right) \left[\frac{E_{\mp}^{\mathrm{b}}(z)}{\tilde{U}_{\mathrm{b}}(1)}\right]\Big|_z & (x-z) \bmod L \in [a,L) \end{cases}
\end{aligned}$$

$w = (x-z) \bmod L$ can also be written as:

$$w = (x-z) \bmod L = \begin{cases} w = x - z & \text{if } x - z \geq 0 \quad \text{(Case 1)} \\ w = x - z + L & \text{if } x - z < 0 \quad \text{(Case 2)} \end{cases}$$

Case a: $(x-z)$ **mod** $L \in [0,a)$

This occurs when:

$$\begin{array}{lll} \text{Case a1} & (x-z \geq 0) \wedge (0 \leq x-z < a) & \Leftrightarrow x - a < z \leq x \\ \text{Case a2} & (x-z < 0) \wedge (0 \leq x-z+L < a) & \Leftrightarrow x + L - a < z \leq x + L \end{array}$$

Case b: $(x-z)$ **mod** $L \in [a,L)$

This occurs when:

$$\begin{array}{lll} \text{Case b1} & (x-z \geq 0) \wedge (a \leq x-z < L) & \Leftrightarrow x - L < z \leq x - a \\ \text{Case b2} & (x-z < 0) \wedge (a \leq x-z+L < L) & \Leftrightarrow x < z \leq x + L - a \end{array}$$

With $z, x \in [0,L]$, the conditions are tightened further:

$$\begin{array}{lll} \text{Case a1} & x - a < z \leq x & \Leftrightarrow \max\{0, x-a\} < z < x \\ \text{Case a2} & x + L - a < z \leq x + L & \Leftrightarrow \min\{L, x+L-a\} < z \leq L \\ \text{Case b1} & x - L < z \leq x - a & \Leftrightarrow 0 < z \leq \max\{0, x-a\} \\ \text{Case b2} & x < z \leq x + L - a & \Leftrightarrow x < z \leq \min\{L, x+L-a\} \end{array}$$

If we now look at the cases $x \in [0, a)$ and $x \in [a, L)$ separately, we can simplify the bounds further:

Case A: $x \in [0, a)$

Case a1	$\max\{0, x-a\} < z < x$	$\Leftrightarrow 0 < z < x$
Case a2	$\min\{L, x+L-a\} < z \leq L$	$\Leftrightarrow x+L-a < z \leq L$
Case b1	$0 < z \leq \max\{0, x-a\}$	$\Leftrightarrow 0 < z \leq 0 = \varnothing$
Case b2	$x < z \leq \min\{L, x+L-a\}$	$\Leftrightarrow x < z \leq x+L-a$

$$
\begin{aligned}
&\int_0^L dz\, \exp\left(\mp\frac{U(x-z)}{D}\right) = \int_{\mathrm{a1}\cup\mathrm{a2}} dz \exp\left(\mp\frac{U_\mathrm{a}(x-z)}{D}\right) + \int_{\mathrm{b1}\cup\mathrm{b2}} dz \exp\left(\mp\frac{U_\mathrm{b}(x-z)}{D}\right) \\
&= \underbrace{\int_0^x dz \exp\left(\mp\frac{U_\mathrm{a}(x-z)}{D}\right)}_{\text{Case a1}} + \underbrace{\int_{x+L-a}^L dz \exp\left(\mp\frac{U_\mathrm{a}(x-z)}{D}\right)}_{\text{Case a2}} + \underbrace{0}_{\text{Case b1}} \\
&\quad + \underbrace{\int_x^{x+L-a} dz \exp\left(\mp\frac{U_\mathrm{b}(x-z)}{D}\right)}_{\text{Case b2}} \\
&= \underbrace{\mp D E^\mathrm{a}_\pm(x) \frac{E^\mathrm{a}_\mp(x)-1}{\tilde{U}_\mathrm{a}(1)}}_{\text{Case a1}} \underbrace{\mp \exp\left(\mp\frac{1}{D}\frac{U_0 L}{a}\right) D E^\mathrm{a}_\pm(x) \frac{E^\mathrm{a}_\mp(L) - E^\mathrm{a}_\mp(x+L-a)}{\tilde{U}_\mathrm{a}(1)}}_{\text{Case a2}} \\
&\quad \underbrace{\mp \exp\left(\pm\frac{1}{D}\frac{U_0 L}{b}\right) D E^\mathrm{b}_\pm(x) \exp\left(\mp\frac{U_0}{D}\left(1+\frac{a}{b}\right)\right) \frac{E^\mathrm{b}_\mp(x+L-a) - E^\mathrm{b}_\mp(x)}{\tilde{U}_\mathrm{b}(1)}}_{\text{Case b2}} \\
&= \mp \frac{D E^\mathrm{a}_\pm(x)}{\tilde{U}_\mathrm{a}(1)} \left[E^\mathrm{a}_\mp(x) - 1 + \exp\left(\mp\frac{1}{D}\frac{U_0 L}{a}\right)\left(E^\mathrm{a}_\mp(L) - E^\mathrm{a}_\mp(x+b)\right)\right] \mp \frac{D}{\tilde{U}_\mathrm{b}(1)}\left[E^\mathrm{b}_\mp(b) - 1\right]
\end{aligned}
$$

with

$$
\exp\left(\pm\frac{U_\mathrm{a}(x)}{D}\right) = \exp\left(\mp\frac{\tilde{U}_\mathrm{a}(x)}{D}\right) = E^\mathrm{a}_\mp(x)
$$

we can simplify:

$$
\begin{aligned}
&\exp\left(\mp\frac{\tilde{U}_\mathrm{a}(x)}{D}\right) \int_0^L dz\, \exp\left(\mp\frac{U(x-z)}{D}\right) \\
&= \mp \frac{D}{\tilde{U}_\mathrm{a}(1)} \left[E^\mathrm{a}_\mp(x) - 1 + \exp\left(\mp\frac{1}{D}\frac{U_0 L}{a}\right)\left(E^\mathrm{a}_\mp(L) - E^\mathrm{a}_\mp(x+b)\right)\right] \mp \frac{D E^\mathrm{a}_\mp(x)}{\tilde{U}_\mathrm{b}(1)}\left[E^\mathrm{b}_\mp(b) - 1\right] \\
&= \mp D E^\mathrm{a}_\mp(x) \left[\frac{1 - \exp\left(\mp\frac{1}{D}\frac{U_0 L}{a}\right) E^\mathrm{a}_\mp(b)}{\tilde{U}_\mathrm{a}(1)} + \frac{E^\mathrm{b}_\mp(b) - 1}{\tilde{U}_\mathrm{b}(1)}\right] \mp D \frac{\exp\left(\mp\frac{1}{D}\frac{U_0 L}{a}\right) E^\mathrm{a}_\mp(L) - 1}{\tilde{U}_\mathrm{a}(1)}
\end{aligned}
$$

Case B: $x \in [a, L)$

$$\begin{array}{lll} \text{Case a1} & \max\{0, x-a\} < z < x & \Leftrightarrow x-a < z < x \\ \text{Case a2} & \min\{L, x+L-a\} < z \leq L & \Leftrightarrow L < z \leq L = \varnothing \\ \text{Case b1} & 0 < z \leq \max\{0, x-a\} & \Leftrightarrow 0 < z \leq x-a \\ \text{Case b2} & x < z \leq \min\{L, x+L-a\} & \Leftrightarrow x < z \leq L \end{array}$$

$$\int_0^L dz\, \exp\left(\pm\frac{U(x-z)}{D}\right) = \int_{\text{a1}\cup\text{a2}} dz \exp\left(\pm\frac{U_\text{a}(x-z)}{D}\right) + \int_{\text{b1}\cup\text{b2}} dz \exp\left(\pm\frac{U_\text{b}(z)}{D}\right)$$

$$= \underbrace{\int_{x-a}^{x} dz \exp\left(\pm\frac{U_\text{a}(x-z)}{D}\right)}_{\text{Case a1}} + \underbrace{0}_{\text{Case a2}} + \underbrace{\int_0^{x-a} dz \exp\left(\pm\frac{U_\text{b}(x-z)}{D}\right)}_{\text{Case b1}} + \underbrace{\int_x^L dz \exp\left(\pm\frac{U_\text{b}(x-z)}{D}\right)}_{\text{Case b2}}$$

$$= \underbrace{\mp D E^\text{a}_\pm(x)) \frac{E^\text{a}_\mp(x) - E^\text{a}_\mp(x-a)}{\tilde{U}_\text{a}(1)}}_{\text{Case a1}} \underbrace{\mp D E^\text{b}_\pm(x)) \exp\left(\mp\frac{U_0}{D}\left(1+\frac{a}{b}\right)\right) \frac{E^\text{b}_\mp(x-a)-1}{\tilde{U}_\text{b}(1)}}_{\text{Case b1}}$$

$$\underbrace{\mp D E^\text{b}_\pm(x)) \exp\left(\pm\frac{1}{D}\frac{U_0 L}{b}\right) \exp\left(\mp\frac{U_0}{D}\left(1+\frac{a}{b}\right)\right) \frac{E^\text{b}_\mp(L) - E^\text{b}_\mp(x)}{\tilde{U}_\text{b}(1)}}_{\text{Case b2}}$$

$$= \mp D \frac{1 - E^\text{a}_\pm(a)}{\tilde{U}_\text{a}(1)} \mp \exp\left(\mp\frac{U_0}{D}\left(1+\frac{a}{b}\right)\right) \frac{D E^\text{b}_\pm(x))}{\tilde{U}_\text{b}(1)} \Bigg[E^\text{b}_\mp(x-a) - 1 +$$

$$+ \exp\left(\pm\frac{1}{D}\frac{U_0 L}{b}\right)\left(E^\text{b}_\mp(L) - E^\text{b}_\mp(x)\right)\Bigg]$$

with

$$\exp\left(\pm\frac{U_\text{b}(x)}{D}\right) = \exp\left(\pm\frac{U_0}{D}\left(1+\frac{a}{b}\right)\right) \exp\left(\mp\frac{\tilde{U}_\text{b}(x)}{D}\right) = \exp\left(\pm\frac{U_0}{D}\left(1+\frac{a}{b}\right)\right) E^\text{b}_\mp(x))$$

we can simplify:

$$\exp\left(\pm\frac{U_\text{b}(x)}{D}\right) \int_0^L dz\, \exp\left(\mp\frac{U(x-z)}{D}\right)$$

$$= \mp \exp\left(\pm\frac{U_0}{D}\left(1+\frac{a}{b}\right)\right) \frac{D E^\text{b}_\mp(x))}{\tilde{U}_\text{a}(1)} \left[1 - E^\text{a}_\pm(a)\right]$$

$$\mp \frac{D}{\tilde{U}_\text{b}(1)} \left[E^\text{b}_\mp(x-a) - 1 + \exp\left(\pm\frac{1}{D}\frac{U_0 L}{b}\right)\left(E^\text{b}_\mp(L) - E^\text{b}_\mp(x)\right)\right]$$

$$= \mp D E^\text{b}_\mp(x)) \left[\frac{E^\text{b}_\pm(a) - \exp\left(\pm\frac{1}{D}\frac{U_0 L}{b}\right)}{\tilde{U}_\text{b}(1)} + \exp\left(\pm\frac{U_0}{D}\left(1+\frac{a}{b}\right)\right) \frac{1 - E^\text{a}_\pm(a)}{\tilde{U}_\text{a}(1)}\right]$$

$$\mp D \frac{\exp\left(\pm\frac{1}{D}\frac{U_0 L}{b}\right) E^\text{b}_\mp(L) - 1}{\tilde{U}_\text{b}(1)}$$

In Summary:

$$I_+(x) = -\begin{cases} E_-^{\mathrm{a}}(x)A_-^{\mathrm{a}} + B_-^{\mathrm{a}} & x \in [0,a) \\ E_-^{\mathrm{b}}(x)A_+^{\mathrm{b}} + B_+^{\mathrm{b}} & x \in [a,L) \end{cases} \tag{B.1}$$

$$I_-(x) = \exp\left(-\frac{i_0 L}{D}\right)\cdot\begin{cases} E_+^{\mathrm{a}}(x)A_+^{\mathrm{a}} + B_+^{\mathrm{a}} & x \in [0,a) \\ E_+^{\mathrm{b}}(x)A_-^{\mathrm{b}} + B_-^{\mathrm{b}} & x \in [a,L) \end{cases} \tag{B.2}$$

with the functions

$$E_\pm^{\mathrm{a,b}}(x) = \exp\left(\pm\frac{U_{\mathrm{a,b}}(x)}{D}\right) \tag{B.3}$$

$$\tilde{U}_{\mathrm{a}}(x) = x\left(i_0 - \frac{U_0}{a}\right) \tag{B.4}$$

$$\tilde{U}_{\mathrm{b}}(x) = x\left(i_0 + \frac{U_0}{b}\right)\ . \tag{B.5}$$

The coefficients are defined by

$$A_\mp^a = \frac{1-\exp\left(\mp\frac{U_0 L}{Da}\right)E_\mp^{\mathrm{a}}(b)}{\tilde{U}_{\mathrm{a}}(1)} + \frac{E_\mp^{\mathrm{b}}(b)-1}{\tilde{U}_{\mathrm{b}}(1)} \tag{B.6}$$

$$B_\mp^a = \frac{\exp\left(\mp\frac{U_0 L}{Da}\right)E_\mp^{\mathrm{a}}(L)-1}{\tilde{U}_{\mathrm{a}}(1)} \tag{B.7}$$

$$A_\pm^b = \exp\left(\pm\frac{U_0}{D}\left(1+\frac{a}{b}\right)\right)\frac{1-E_\pm^{\mathrm{a}}(a)}{\tilde{U}_{\mathrm{a}}(1)} + \frac{E_\pm^{\mathrm{b}}(a)-\exp\left(\pm\frac{U_0 L}{Db}\right)}{\tilde{U}_{\mathrm{b}}(1)} \tag{B.8}$$

$$B_\pm^b = \frac{\exp\left(\pm\frac{U_0 L}{Db}\right)E_\pm^{\mathrm{b}}(-L)-1}{\tilde{U}_{\mathrm{b}}(1)}\ . \tag{B.9}$$

Acknowledgements

First of all, I want to thank Prof. Fabian Hassler for making this thesis possible and introducing me to this exciting branch of physics. His guidance has not only deepened my understanding of the subject, but also my enthusiasm for academia.

I firmly thank David Scheer for always being available for questions and discussions. I have always gained valuable knowledge and insights from our conversations.

In addition, I am thankful for all the people at the Institute for Quantum Information for the nice environment at the office.

Furthermore, I am grateful for my girlfriend Lieke De Gans for her love and support during this time, and my good friend Andrey Lekov for proofreading my work.

Bibliography

[1] V. Balakrishnan. *Elements of Nonequilibrium Statistical Mechanics*. 1st ed. Engineering. Under exclusive license to Springer Nature Switzerland AG. Cham: Springer Cham, 2021, pp. XIX, 314. ISBN: 978-3-030-62233-6. DOI: 10.1007/978-3-030-62233-6.

[2] Andre C. Barato and Udo Seifert. "Thermodynamic Uncertainty Relation for Biomolecular Processes". In: *Phys. Rev. Lett.* 114 (15 Apr. 2015), p. 158101. DOI: 10.1103/PhysRevLett.114.158101.

[3] Alexander M. Berezhkovskii and Leonardo Dagdug. "Biased diffusion in periodic potentials: Three types of force dependence of effective diffusivity and generalized Lifson-Jackson formula". In: *The Journal of Chemical Physics* 151.13 (Oct. 2019). 6 pages, p. 131102. DOI: 10.1063/1.5120279.

[4] A. Mert Bozkurt et al. "Double-Fourier engineering of Josephson energy-phase relationships applied to diodes". In: *SciPost Phys.* 15 (2023), p. 204. DOI: 10.21468/SciPostPhys.15.5.204.

[5] M. Büttiker. "Transport as a consequence of state-dependent diffusion". In: *Zeitschrift für Physik B Condensed Matter* 68.2 (June 1987), pp. 161–167. ISSN: 1431-584X. DOI: 10.1007/BF01304221.

[6] Boris Chesca, Reinhold Kleiner, and Dieter Koelle. "SQUID Theory". In: *The SQUID Handbook*. John Wiley and Sons, Ltd, 2004. Chap. 2, pp. 29–92. ISBN: 9783527603640. DOI: https://doi.org/10.1002/3527603646.ch2. eprint: https://onlinelibrary.wiley.com/doi/pdf/10.1002/3527603646.ch2.

[7] Todd R. Gingrich et al. "Dissipation Bounds All Steady-State Current Fluctuations". In: *Phys. Rev. Lett.* 116 (12 Mar. 2016), p. 120601. DOI: 10.1103/PhysRevLett.116.120601.

[8] Geoffrey Grimmett and David Stirzaker. *Probability and random processes*. Oxford; New York: Oxford University Press, 2001. ISBN: 0198572239.

[9] Yoshihiko Hasegawa and Tan Van Vu. "Uncertainty relations in stochastic processes: An information inequality approach". In: *Phys. Rev. E* 99 (6 June 2019), p. 062126. DOI: 10.1103/PhysRevE.99.062126.

[10] Kumiko Hayashi and Shin-ichi Sasa. "Effective temperature in nonequilibrium steady states of Langevin systems with a tilted periodic potential". In: *Phys. Rev. E* 69 (6 June 2004), p. 066119. DOI: 10.1103/PhysRevE.69.066119.

[11] Desmond J. Higham. "An Algorithmic Introduction to Numerical Simulation of Stochastic Differential Equations". In: *SIAM Review* 43.3 (2001), pp. 525–546. DOI: 10.1137/S0036144500378302. eprint: https://doi.org/10.1137/S0036144500378302.

[12] Jordan M. Horowitz and Todd R. Gingrich. "Thermodynamic uncertainty relations constrain non-equilibrium fluctuations". In: *Nature Physics* 16 (2020), pp. 15–20. DOI: 10.1038/s41567-019-0702-6.

[13] Jens Koch et al. "Charge-insensitive qubit design derived from the Cooper pair box". In: *Phys. Rev. A* 76 (4 Oct. 2007), p. 042319. DOI: 10.1103/PhysRevA.76.042319.

[14] Timur Koyuk and Udo Seifert. "Thermodynamic Uncertainty Relation in Interacting Many-Body Systems". In: *Phys. Rev. Lett.* 129 (21 Nov. 2022), p. 210603. DOI: 10.1103/PhysRevLett.129.210603.

[15] Oliver Niggemann and Udo Seifert. "Field-Theoretic Thermodynamic Uncertainty Relation". In: *Journal of Statistical Physics* 178 (2020), pp. 1142–1174. DOI: 10.1007/s10955-019-02479-x.

[16] P. Reimann et al. "Diffusion in tilted periodic potentials: Enhancement, universality, and scaling". In: *Phys. Rev. E* 65 (3 Feb. 2002), p. 031104. DOI: 10.1103/PhysRevE.65.031104.

[17] Peter Reimann. "Brownian motors: noisy transport far from equilibrium". In: *Physics Reports* 361.2 (2002), pp. 57–265. ISSN: 0370-1573. DOI: https://doi.org/10.1016/S0370-1573(01)00081-3.

[18] Hannes Risken. *The Fokker-Planck Equation: Methods of Solution and Applications*. 2nd ed. Springer Series in Synergetics. 3 b/w illustrations. Springer Berlin, Heidelberg, 1996, pp. XIV, 472. ISBN: 978-3-540-61530-9. DOI: 10.1007/978-3-642-61544-3.

[19] V. M. Rozenbaum et al. "Exactly solvable model of a slightly fluctuating ratchet". In: *Phys. Rev. E* 104 (1 July 2021), p. 014133. DOI: 10.1103/PhysRevE.104.014133.

[20] Kazuo Sasaki and Satoshi Amari. "Diffusion Coefficient and Mobility of a Brownian Particle in a Tilted Periodic Potential". In: *Journal of the Physical Society of Japan* 74.8 (2005), pp. 2226–2232. DOI: 10.1143/JPSJ.74.2226. eprint: https://doi.org/10.1143/JPSJ.74.2226.

[21] David Scheer, Jonas Völler, and Fabian Hassler. "The superconducting clock-circuit: Improving the coherence of Josephson radiation beyond the thermodynamic uncertainty relation". In: *SciPost Phys.* 17 (2024), p. 140. DOI: 10.21468/SciPostPhys.17.5.140.

[22] T. Scheller et al. "SNS Junctions for AC Josephson Voltage Standards". In: *Physics Procedia* 36 (2012). SUPERCONDUCTIVITY CENTENNIAL Conference 2011, pp. 48–52. ISSN: 1875-3892. DOI: https://doi.org/10.1016/j.phpro.2012.06.128.

[23] Francesco Tafuri, ed. *Fundamentals and Frontiers of the Josephson Effect.* 1st ed. Vol. 286. Springer Series in Materials Science. Springer Nature Switzerland AG. Springer Cham, 2019, pp. XXXVIII, 859. ISBN: 978-3-030-20726-7. DOI: 10.1007/978-3-030-20726-7.